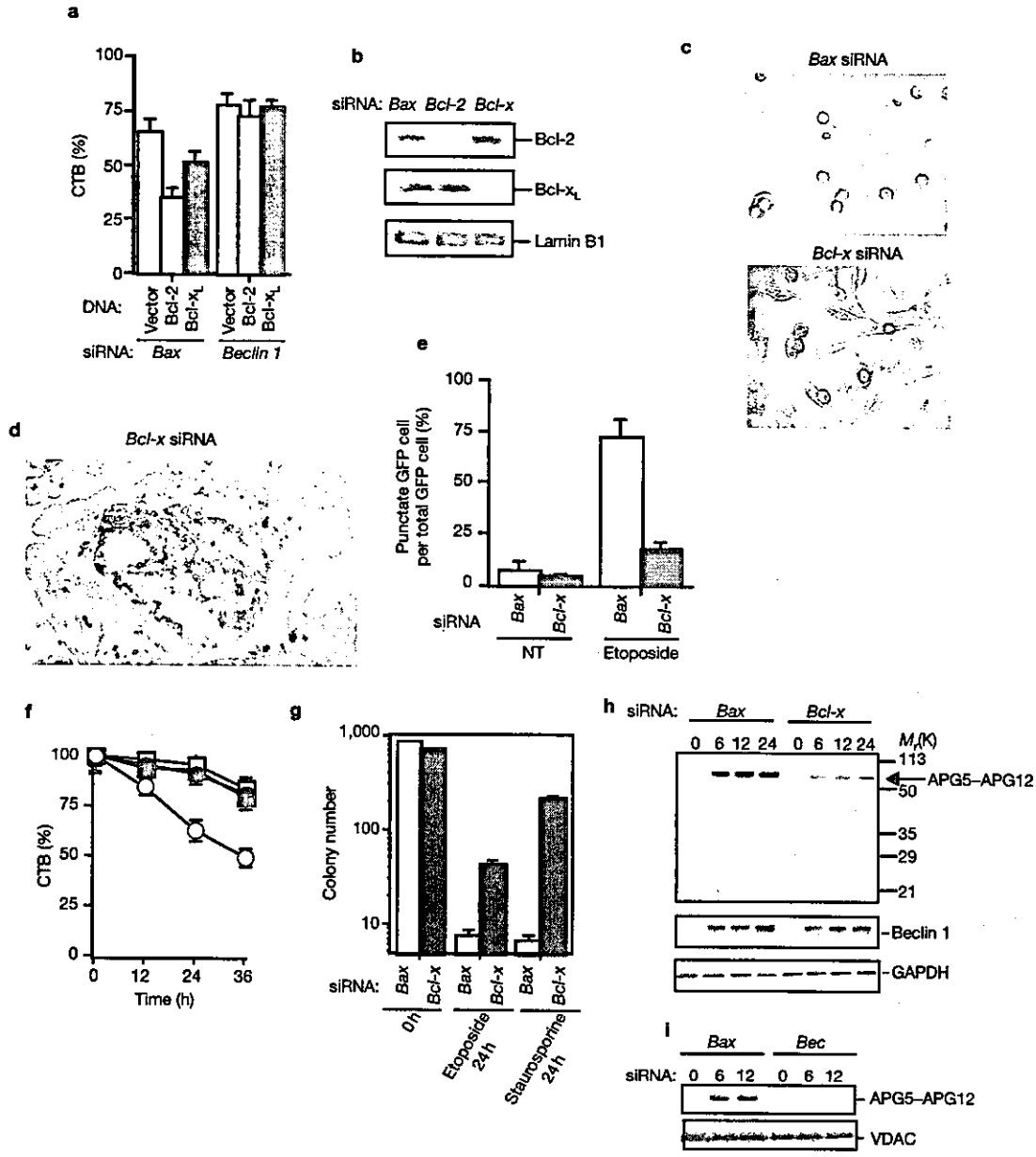

Figure 5 Inhibition of non-apoptotic death in etoposide-treated Bax/Bak$^{-/-}$ MEFs by siRNA for Bcl-x. (**a**) Enhancement of etoposide-induced non-apoptotic death by overexpression of human Bcl-2 and Bcl-x_L in Bax/Bak$^{-/-}$ MEFs in a Beclin 1-dependent manner. Bax/Bak$^{-/-}$ MEFs with silencing of control Bax or Beclin 1 were transfected with the indicated plasmids (1 μg). After 24 h, the transfected cells were incubated with 20 μM etoposide for 24 h, and cell viability was assessed by the CTB assay. Data are shown as mean ± s.d. ($n = 3$). (**b**) Bax/Bak$^{-/-}$ MEFs were transiently transfected with 10 μg of siRNA for Bcl-2, Bcl-x, or Bax (negative control) for 24 h. Expression levels of Bcl-2, Bcl-x_L and Lamin B (loading control) were analysed by Western blot analysis. (**c–e**) Inhibition of etoposide-induced autophagy in Bax/Bak$^{-/-}$ cells treated with siRNA for Bcl-x. (**c**) Bax/Bak$^{-/-}$ MEFs that were transfected with the indicated siRNAs were treated with 20 μM etoposide for 24 h, then examined by phase-contrast microscopy. (**d**) Bax/Bak$^{-/-}$ MEFs that were transfected with siRNA for Bcl-x and then treated with etoposide for 18 h were analysed by electron microscopy (×8,500). (**e**) Reduction of punctate GFP–LC3 fluorescence in etoposide-treated Bax/Bak$^{-/-}$ MEFs by silencing of Bcl-x. Bax/Bak$^{-/-}$ MEFs that were transfected with both GFP–LC3 and the indicated siRNAs were incubated without (NT) or with etoposide for 24 h, and then were examined by confocal fluorescent microscopy. The percentage of cells with punctate GFP–LC3 fluorescence was calculated relative to all GFP–LC3-positive cells. $n = 4$. (**f**) Inhibition of etoposide-induced cell death by silencing of Bcl-x. Bax/Bak$^{-/-}$ MEFs were transfected with siRNA (circles, siRNA for Bax; squares, siRNA for Bcl-x) were treated with 20 μM etoposide in the absence (open symbols) or presence (closed symbols) of 10 mM 3-MA, and cell viability was assessed by the CTB assay at the indicated times. $n = 4$. (**g**) Clonogenicity assay of Bax/Bak$^{-/-}$ MEFs after exposure to etoposide and staurosporine. Bax/Bak$^{-/-}$ MEFs that were transfected with the indicated siRNAs were treated with 20 μM etoposide or 1 μM staurosporine at 24 h. After collection, 2,000 cells were seeded in the normal medium. After one week, colonies were counted. (**h, i**) Inhibition of APG5–APG12 induction by silencing of Bcl-x or Beclin 1. Bax/Bak$^{-/-}$ MEFs were treated with the indicated siRNAs (10 μg) for 24 h and then incubated with 20 μM etoposide for the indicated times. Expression of APG5–APG12 complex, Beclin 1 and GAPDH/VDAC (loading control) was analysed by Western blot analysis.

Bcl-x_L-expressing plasmid and then treated with etoposide. As shown in Fig. 4d, the viability of Bcl-x_L-expressing *APG5*$^{-/-}$ MEFs was superior to that of Bcl-x_L-expressing *APG5*$^{+/+}$ MEFs, and the latter was increased by 3-MA. In both types of cells, apoptosis was similarly inhibited (Fig. 4e). Thus, whereas overexpression of Bcl-x_L clearly increased the survival of both *APG5*$^{+/+}$ and *APG5*$^{-/-}$ cells, Bcl-x_L overexpression increased the difference in cell death between *APG5*$^{+/+}$ and *APG5*$^{-/-}$ cells, which would be predicted to be the autophagic component. In contrast to Bcl-x_L, vector DNA transfection did not produce any difference between the viability of *APG5*$^{-/-}$ MEFs and *APG5*$^{+/+}$ MEFs, irrespective of the presence of zVAD-fmk (Fig. 4d). Similar findings were obtained when Bcl-2-expressing plasmid was used (data not shown). Non-apoptotic death observed in MEFs with overexpressed Bcl-2/Bcl-x_L was not seen when Beclin 1 was silenced (Fig. 4f). These data suggested that overexpression of Bcl-2 or Bcl-x_L not only inhibited apoptosis, but also sensitized at least a fraction of cells to non-apoptotic death dependent on autophagy genes (such as Bax/Bak-deficiency); however, we could not formally exclude the possibility that overexpression of Bcl-2 and Bcl-x_L simply increases the efficiency of autophagosome formation, which may not necessarily be translated into more cell death, and that APG5 and Beclin 1 are relevant modulators of cell death.

In the *Bax/Bak*$^{-/-}$ cells, apoptotic reagents induced non-apoptotic cell death, which was dependent on genes related to autophagy, including Beclin 1. Beclin 1 interacts with Bcl-2/Bcl-x_L (but not Bax/Bak)[12], raising the possibility that Bcl-2/Bcl-x_L may have a role in the non-apoptotic death of *Bax/Bak*$^{-/-}$ MEFs. We first examined the effect of overexpression of Bcl-2 and Bcl-x_L in *Bax/Bak*$^{-/-}$ MEFs. As expected, overexpression of Bcl-2 and Bcl-x_L in *Bax/Bak*$^{-/-}$ MEFs resulted in enhancement of the non-apoptotic death, which was cancelled by silencing of Beclin 1 (Fig. 5a). We next examined the effect of silencing these molecules in *Bax/Bak*$^{-/-}$ MEFs by using siRNA. Endogenous Bcl-2 and Bcl-x_L were almost completely eliminated from *Bax/Bak*$^{-/-}$ MEFs by the respective siRNAs (Fig. 5b). Despite etoposide treatment, a large fraction of the Bcl-x-silenced *Bax/Bak*$^{-/-}$ MEFs appeared healthy (Fig. 5c) and the creation of autophagosomes was markedly suppressed (Fig. 5d, e). The majority of the cells remained viable irrespective of the addition of 3-MA (Fig. 5f), indicating that the non-apoptotic death was not induced and suggesting that Bcl-x_L was required for the non-apoptotic death of *Bax/Bak*$^{-/-}$ MEFs. As expected in the absence of Bax/Bak, these cells did not undergo apoptotic death (data not shown). In contrast to the silencing of Bcl-x, silencing of Bcl-2 did not have any effect (see Supplementary Information, Fig. S2j, k)—probably not owing to functional differences between Bcl-2 and Bcl-x, but to the much lower level of Bcl-2 than Bcl-x_L expression in MEFs—because Bcl-2 overexpression cancelled the effect of Bcl-x silencing (see Supplementary Information, Fig. S2l). The improved viability after Bcl-x silencing was also confirmed by a clonogenicity assay (Fig. 5g). As shown in Fig. 5h, the etoposide-induced increase of Beclin 1 in Bcl-x-silenced *Bax/Bak*$^{-/-}$ MEFs was similar to that in control *Bax/Bak*$^{-/-}$ MEFs, whereas induction of APG5–APG12 was far weaker in Bcl-x-silenced *Bax/Bak*$^{-/-}$ MEFs than in control *Bax/Bak*$^{-/-}$ MEFs. Because Beclin 1 binds to Bcl-x_L, and silencing of Beclin 1 reduced the APG5–APG12 level (Fig. 5i), Bcl-x_L might be required for induction of APG5–APG12 through regulation of Beclin 1.

Because *Bax/Bak*$^{-/-}$ MEFs lost viability after exposure to apoptotic stimuli in an autophagic protein-dependent and 3-MA-inhibitable manner, it might be assumed that this type of non-apoptotic death is similar to death induced by nutrient starvation, which also activates the autophagic process. However, etoposide/staurosporine-induced non-apoptotic death of *Bax/Bak*$^{-/-}$ cells showed substantial differences from death induced by amino-acid starvation on the basis of the following findings: (1) whereas etoposide/staurosporine-induced non-apoptotic death of *Bax/Bak*$^{-/-}$ is inhibited by 3-MA, amino-acid starvation-induced death is not inhibited, but rather is enhanced by 3-MA (see Supplementary Information, Fig. S3a, b), probably owing to an impaired supply of amino acids; (2) amino-acid starvation induces apoptosis in WT cells that are dependent on Bax/Bak (see Supplementary Information, Fig. S3b); and (3) accumulation of Beclin 1 and APG5–APG12 was observed in cells undergoing etoposide/staurosporine-induced non-apoptotic death, but not in cells that died of amino-acid starvation (see Supplementary Information, Fig. S3c). Thus, the non-apoptotic death of *Bax/Bak*$^{-/-}$ MEFs occurs in a different manner from starvation-induced cell death. Furthermore, although autophagic proteins are required, their role shows considerable differences between nutrient starvation and non-apoptotic death of *Bax/Bak*$^{-/-}$ cells.

Non-apoptotic (type II-like) death was observed in *Bax/Bak*$^{-/-}$ MEFs irrespective of their immortalization and was also seen in *Bax/Bak*$^{-/-}$ thymocytes. However, whether other normal cells also have the potential to undergo type II-like death requires further investigation. Among the cultured cell lines tested so far, overexpression of Bcl-2 did not sensitize HeLa, Jurkat or HCT116 cells to etoposide-induced non-apoptotic death (data not shown). Non-apoptotic death potential could be restricted to certain cells in the *in vitro* setting. As previously suggested[10], many cancer cells might have lost the ability to undergo non-apoptotic death as a growth advantage.

How does the Bcl-2 family of proteins regulate the non-apoptotic death? Overexpression of proteins in the BH (Bcl-2 homology) 3 subfamily (BH3-only proteins) did not induce the non-apoptotic death in *Bax/Bak*$^{-/-}$ MEFs (see Supplementary Information, Fig. S4), indicating that activation of BH3-only proteins is not sufficient to produce this form of cell death. Because Beclin 1 is required for the non-apoptotic death of *Bax/Bak*$^{-/-}$ cells and because Bcl-2/Bcl-x_L (but not Bax/Bak) binds to Beclin 1 (ref. 12), Bcl-2/Bcl-x_L might influence the creation of autophagosomes at least partly by regulation of Beclin 1. This notion is supported by the fact that the apoptotic stimulus-dependent increase of APG5–APG12 in *Bax/Bak*$^{-/-}$ MEFs (which was regulated by Beclin 1) was markedly reduced by silencing Bcl-x. This hypothesis certainly needs to be tested by using mutants of Bcl-2/Bcl-x_L and Beclin 1 that fail to interact with each other.

Anti-apoptotic Bcl-2/Bcl-x_L and pro-apoptotic Bax/Bak regulate apoptosis in opposite directions by acting on each other as well as by influencing other molecules, so the balance between these proteins is a crucial determinant of whether or not apoptosis occurs[3]. The fact that *Bax/Bak*$^{-/-}$ MEFs, in which anti-apoptotic Bcl-2 family members dominate over pro-apoptotic members, and Bcl-2/Bcl-x_L-overexpressing MEFs undergo the non-apoptotic death, suggests that the balance between Bcl-2/Bcl-x_L and Bax/Bak is also crucial for determining the occurrence of the non-apoptotic death. It has previously been described that some Bcl-2 family members can reverse their death-regulating activities, depending on expression levels or cellular contexts[13–16]. Overexpression of Bcl-2 has been reported to promote cell death from different mechanisms, for example, via proteolytic cleavage with caspases[15] or via interaction with an orphan nuclear receptor Nur77 (ref. 16). Therefore, the possibility was not formally excluded that an important role of Bcl-2/Bcl-x_L in the non-apoptotic death is dependent on this cryptic pro-death activity.

In conclusion, these findings demonstrate a previously unknown role of the Bcl-2 family in the regulation of non-apoptotic (type II-like) programmed cell death, in addition to the well-known role of this protein family in apoptosis. □

METHODS

Antibodies and chemicals. Anti-mouse Bcl-2, anti-Beclin 1 and anti-GAPDH (6G7) monoclonal antibodies were obtained from BD Biosciences (San Jose, CA). Anti-Lamin B1 and anti-VDAC monoclonal antibodies were purchased from Zymed (San Francisco, CA) and Calbiochem (La Jolla, CA), respectively. Anti-Bcl-x (L-19) polyclonal antibody was obtained from Santacruz Biotechnology (Santa Cruz, CA). Anti-APG5 polyclonal antibody was described previously[9]. 3-MA and Cell Titer Blue were obtained from ICN Biochemicals (Irvine, CA) and Promega (Madison, WI), respectively. Other chemicals were purchased from Wako (Osaka, Japan).

Cell culture and DNA transfection. Primary and SV40 T antigen-transformed WT and *Bax/Bak*$^{-/-}$ MEFs were grown in Dulbecco's modified Eagle's medium (DMEM). Apaf-1-deficient and caspase-9-deficient MEFs and their control MEFs (provided by X. Wang and K. Kuida, respectively) were also grown in the same medium. DNAs encoding human Bax, human Bak, human Bcl-2 and human Bcl-x_L in the pUC-CAGGS expression vector[17] were used. The GFP–LC3 expression construct was described elsewhere[8]. Cells (1×10^6) were transfected with plasmid DNA using the Amaxa electroporation system according to the supplier's protocol (kit V, program U-20). The transfection efficiency was more than 75% as assessed by co-transfection with DNA expressing GFP. All the siRNAs were produced by Dharmacon Research. The sequences used were as follows (numbers in parentheses indicate nucleotide positions within the respective open reading frame): mouse *Bcl-x* siRNA, 5′-AAGGAUACAGCUGGAGUCAGU-3′ (59–79); mouse *Bcl-2* siRNA, 5′-AAGUACAUACAUUAUAAGCUG-3′ (49–69); mouse *Bax* siRNA, 5′-AACAGAUCAUGAAGACAGGGG-3′ (50–70); mouse *Beclin 1* siRNA, 5′-AAGAUCCUGGACCGGGUCACC-3′ (91–111); mouse *APG5* siRNA, 5′-AACUUGCUUUACUCUCUCUAUCA-3′ (51–71). Cells (1×10^6) were transfected with 10 μg of siRNA using the Amaxa electroporation system. In the case of transfection with complementary DNA and siRNA, cDNAs (1 μg) were transfected, and after 24 h siRNAs (10 μg) were introduced.

Cell viability assay. Cells (3.5×10^6 per well) were seeded into 6-well dishes. After 24 h, the cells were treated with etoposide (20 μM) or staurosporine (1 μM) in the presence or absence of zVAD-fmk (100 μM) or 3-MA (10 mM). PI (2 μM) was added into the medium, and cells were observed under a BX50 fluorescence microscope (Olympus, Tokyo, Japan). In another experiments, all of the cells, including floating cells, were collected and viability was assessed by nuclear morphology after Hoechst 33342 (Ho342) staining, or the CTB assay. Briefly, cells were stained with 1 μM Ho342 for 5 min at room temperature, and were analysed with a fluorescence microscope (Olympus, BX50). The CTB assays were performed using CTB assay reagent, according to the supplier's protocols.

To examine the proliferation ability, MEFs were treated with etoposide or staurosporine, all the cells were recovered and 5,000 or 10,000 cells were re-cultured in standard medium into 96-well or 48-well dishes, respectively. Viable cell numbers were measured on the indicated days by the CTB assay. In the clonogenicity assay, MEFs were treated with etoposide or staurosporine, collected, and 2,000 cells were seeded in standard medium into 24-well dishes. After one week, colony numbers were counted.

Staining of autophagosomes. Cells were transfected with 1 μg of GFP–LC3 expression plasmid[8]. After 24 h, cells were treated with etoposide or staurosporine, and the fluorescence of GFP–LC3 was observed under a confocal fluorescence microscope (LSM 510 META, Zeiss, Thornwood, NY).

Electron microscopy. Cells were fixed with 2% paraformaldehyde/2% glutaraldehyde in 0.1 M phosphate buffer (pH 7.4), followed by 1% OsO_4. After dehydration, thin sections were stained with uranyl acetate and lead citrate for observation under a JEM 100 CX electron microscope (JEOL, Peabody, MA).

Note: Supplementary Information, Information is available on the Nature Cell Biology website.

ACKNOWLEDGEMENTS

We are grateful to S. J. Korsmeyer for providing SV40-immortalized *Bax/Bak*$^{-/-}$ MEFs. This study was supported in part by grants for Scientific Research on Priority Areas, Center of Excellence Research, the twenty-first century COE Program, and Scientific Research, from the Ministry of Education, Science, Sports and Culture of Japan, and by a grant for Research on Dementia and Fracture from the Ministry of Health, Labour and Welfare of Japan.

COMPETING FINANCIAL INTERESTS

The authors declare that they have no competing financial interests.

Received 12 July 2004; accepted 5 October 2004
Published online at http://www.nature.com/naturecellbiology.

1. Baehrecke, E. H. How death shapes life during development. *Nature Rev. Mol. Cell Biol.* **3,** 779–787 (2002).
2. Clarke, P. G. Developmental cell death: morphological diversity and multiple mechanisms. *Anat. Embryol. (Berl.)* **181,** 195–213 (1990).
3. Tsujimoto, Y. Cell death regulation by the Bcl-2 protein family in the mitochondria. *J. Cell. Physiol.* **195,** 158–167 (2003).
4. Lindsten, T. *et al.* The combined functions of proapoptotic Bcl-2 family members bak and bax are essential for normal development of multiple tissues. *Mol. Cell* **6,** 1389–1399 (2000).
5. Wei, M. C. *et al.* Proapoptotic BAX and BAK: a requisite gateway to mitochondrial dysfunction and death. *Science* **292,** 727–730 (2001).
6. Zong, W. X., Lindsten, T., Ross, A. J., MacGregor, G. R. & Thompson, C. B. BH3-only proteins that bind pro-survival Bcl-2 family members fail to induce apoptosis in the absence of Bax and Bak. *Genes Dev.* **15,** 1481–1486 (2001).
7. Bursch, W. The autophagosomal-lysosomal compartment in programmed cell death. *Cell Death Differ.* **8,** 569–581 (2001).
8. Kabeya, Y. *et al.* LC3, a mammalian homologue of yeast Apg8p, is localized in autophagosome membranes after processing. *EMBO J.* **19,** 5720–5728 (2000).
9. Mizushima, N. *et al.* Dissection of autophagosome formation using Apg5-deficient mouse embryonic stem cells. *J. Cell Biol.* **152,** 657–668 (2001).
10. Liang, X. H. *et al.* Induction of autophagy and inhibition of tumorigenesis by beclin 1. *Nature* **402,** 672–676 (1999).
11. Kihara, A., Kabeya, Y., Ohsumi, Y. & Yoshimori, T. Beclin-phosphatidylinositol 3-kinase complex functions at the trans-Golgi network. *EMBO Rep.* **2,** 330–335 (2001).
12. Liang, X. H. *et al.* Protection against fatal Sindbis virus encephalitis by beclin, a novel Bcl-2-interacting protein. *J. Virol.* **72,** 8586–8596 (1998).
13. Chen, J. *et al.* bcl-2 overexpression reduces apoptotic photoreceptor cell death in three different retinal degenerations. *Proc. Natl Acad. Sci. USA* **93,** 7042–7047 (1996).
14. Fannjiang, Y. *et al.* BAK alters neuronal excitability and can switch from anti- to pro-death function during postnatal development. *Dev. Cell* **4,** 575–585 (2003).
15. Cheng, E. H. *et al.* Conversion of Bcl-2 to a Bax-like death effector by caspases. *Science* **278,** 1966–1968 (1997).
16. Lin, B. *et al.* Conversion of Bcl-2 from protector to killer by interaction with nuclear orphan receptor Nur77/TR3. *Cell* **116,** 527–540 (2004).
17. Shimizu, S., Eguchi, Y., Kamiike, W., Matsuda, H. & Tsujimoto, Y. Bcl-2 expression prevents activation of the ICE protease cascade. *Oncogene* **12,** 2251–2257 (1996).
18. Kuma, A. *et al.* The role of autophagy during the early neonatal starvation period. *Nature* (in the press).

THE JOURNAL OF BIOLOGICAL CHEMISTRY
Vol. 279, No. 50, Issue of December 10, pp. 52726–52734, 2004
Printed in U.S.A.

Fzo1, a Protein Involved in Mitochondrial Fusion, Inhibits Apoptosis*

Received for publication, August 4, 2004, and in revised form, September 28, 2004
Published, JBC Papers in Press, September 30, 2004, DOI 10.1074/jbc.M408910200

Rie Sugioka, Shigeomi Shimizu, and Yoshihide Tsujimoto‡

From the Laboratory of Molecular Genetics, Department of Post-Genomics & Diseases, Osaka University Medical School, and Solution-Oriented Research for Science and Technology of Japan Science and Technology Corporation, 2-2 Yamadaoka, Suita, Osaka 565-0871, Japan

Mitochondrial morphology and physiology are regulated by the processes of fusion and fission. Some forms of apoptosis are reported to be associated with mitochondrial fragmentation. We showed that overexpression of Fzo1A/B (rat) proteins involved in mitochondrial fusion, or silencing of Dnm1 (rat)/Drp1 (human) (a mitochondrial fission protein), increased elongated mitochondria in healthy cells. After apoptotic stimulation, these interventions inhibited mitochondrial fragmentation and cell death, suggesting that a process involved in mitochondrial fusion/fission might play a role in the regulation of apoptosis. Consistently, silencing of Fzo1A/B or Mfn1/2 (a human homolog of Fzo1A/B) led to an increase of shorter mitochondria and enhanced apoptotic death. Overexpression of Fzo1 inhibited cytochrome *c* release and activation of Bax/Bak, as assessed from conformational changes and oligomerization. Silencing of Mfn or Drp1 caused an increase or decrease of mitochondrial sensitivity to apoptotic stimulation, respectively. These results indicate that some of the proteins involved in mitochondrial fusion/fission modulate apoptotic cell death at the mitochondrial level.

Apoptosis plays an important role in various biological events in metazoans, including development and maintenance of tissue homeostasis. A family of cysteine proteases called caspases cleaves various cellular proteins and thus drives the process of apoptosis. It has been shown that the mitochondria play a pivotal role in apoptosis by releasing several apoptogenic molecules (such as cytochrome *c*, Smac/DIABLO, Omi/HtrA2, AIF, and endonuclease G) into the cytoplasm from the intermembrane space, after which these molecules activate downstream destruction programs, including the caspase cascade (1). The pro-apoptotic increase of mitochondrial membrane permeability is mainly regulated by members of the Bcl-2 family of proteins (2–4). Bcl-2 family consists of anti-apoptotic members such as Bcl-2 as well as pro-apoptotic members, including multidomain members such as Bax and Bak and numerous BH3-only proteins (*e.g.* Bid). BH3-only proteins, when activated, transmit apoptotic signals to the mitochondria to activate Bax and Bak (which act as a gateway), leading to mitochondrial membrane permeabilization (5, 6). The apoptotic mitochondrial membrane permeabilization may also be influenced by the mitochondrial physiological status, including respiration, lipid context, and fusion/fission (7).

Mitochondria are continuously fusing and dividing, processes that are thought to have a role in homeostasis. In *Saccharomyces cerevisiae*, fission of the outer mitochondrial membrane is driven by Dnm1p, Fis1p, and Mdv1p (8–10), whereas Mdm33p is involved in fission of the inner mitochondrial membrane (11). Dnm1p is a dynamin-related GTPase that is normally localized in the cytosol (8); it undergoes translocation and binds to the outer membrane via Fis1p during fission (9) and is thought to form a large oligomeric ring-like complex that pinches the outer mitochondrial membrane. Deletion of any of the fission genes blocks mitochondrial fission and produces a fused, interconnected mitochondrial network. Orthologs of Dnm1p have been characterized in *Caenorhabditis elegans* (DRP1) (12) as well as in mammals (Drp1) (13). Fzo1p and Ugo1p drive fusion of the outer mitochondrial membrane (14–16), whereas Mgm1p is involved in fusion of the inner mitochondrial membrane (17) in *S. cerevisiae*. Fzo1 was first characterized in *Drosophila melanogaster* and is a large GTPase that circumscribes the outer membrane and is essential for mitochondrial fusion (18). Mutations of the *fzo* gene in flies inhibit mitochondrial fusion during spermatogenesis, leading to a "fuzzy onion" morphology (18). A homolog of Fzo1 protein is found in mammals (*e.g.* rat Fzo1 and human Mfn) (19, 20). Defects of yeast fzo1 or the mammalian homologs of Fzo1 result in extensive fragmentation of the mitochondria and lead to cells being classed as the ρ^0 phenotype, which lacks mitochondrial DNA (14).

Recent studies have suggested that the processes of mitochondrial fusion/fission are somehow involved in the regulation of apoptosis. During the early stage of apoptosis, the mitochondrial network is destroyed in mammalian cells (21–23). It has also been shown that overexpression of a dominant-negative Drp1 mutant (Drp1K38A) prevents apoptotic fragmentation of the mitochondrial network, as well as the occurrence of cytochrome *c* release, and apoptosis (21). Furthermore, silencing of Opa1 (a human homolog of Mgm1p) and overexpression of Fis1 both induce mitochondrial fragmentation, and reportedly also induce apoptosis (24, 25). However, the mechanisms by which fusion and fission processes are involved in apoptosis remain to be elucidated.

In the present study, we confirmed that mitochondrial fragmentation occurred during apoptosis in some cell lines. We also found that increasing or decreasing the expression of proteins involved in mitochondrial fusion (Fzo1/Mfn) relative to proteins involved in fission (Dnm1/Drp1) resulted in cells becoming more resistant or more sensitive to apoptotic stimulation, re-

* This work was supported in part by a grant for Scientific Research on Priority Areas, by a grant for Center of Excellence Research, a grant for the 21st century COE Program, by a grant for Scientific Research from the Ministry of Education, Science, Sports and Culture, and by a grant for Research on Dementia and Fracture from the Ministry of Health, Labor and Welfare of Japan. The costs of publication of this article were defrayed in part by the payment of page charges. This article must therefore be hereby marked "*advertisement*" in accordance with 18 U.S.C. Section 1734 solely to indicate this fact.

‡ To whom correspondence should be addressed. Tel.: 81-6-6879-3363; Fax: 81-6-6879-3369; E-mail: tsujimot@gene.med.osaka-u.ac.jp.

spectively, by influencing the activation of Bax/Bak in the mitochondria.

EXPERIMENTAL PROCEDURES

Chemicals and Antibodies—Bismaleimidohexane was obtained from Pierce. The caspase inhibitor z-VAD-fmk[1] was purchased from Peptide Inc. (Minoh, Japan).

An anti-Bax polyclonal antibody (N-20) and anti-Bak monoclonal antibody (Ab-1) were obtained from Santa Cruz Biotechnology (Santa Cruz, CA) and Oncogene (Boston, MA), respectively. Anti-Drp1 and anti-Tom20 monoclonal antibodies were purchased from Transduction Laboratory (San Diego, CA). Anti-human Fas monoclonal antibody (CH-11), anti-cytochrome *c* (6H2 and 7H8) monoclonal antibodies, and goat anti-mouse Alexa Fluor 488 antibody were obtained from MBL (Nagoya, Japan), BD Pharmingen, and Molecular Probes (Eugene, OR), respectively. Anti-GAPDH antibody and anti-porin (voltage-dependent anion channel) monoclonal antibody were purchased from Chemicon (Temecula, CA) and Calbiochem, respectively.

Cell Culture and DNA Transfection—HeLa cells (a human cervical carcinoma cell line) and a derivative cell line with stable overexpression of human Bcl-2 (26) were maintained in RPMI1640 medium supplemented with 10% fetal bovine serum. Rat1 cells (a rat fibroblast cell line) were grown in Dulbecco's modified Eagle's medium supplemented with 10% fetal bovine serum. SV40 T antigen-transformed wild type (WT) and Bax/Bak double knockout MEFs were grown in modified Dulbecco's modified Eagle's medium containing 10% fetal bovine serum.

To visualize mitochondria in living cells, DNA encoding Su9-DsRed2 was used: this fusion construct was produced by insertion of the presequence of mouse F_1F_0 ATPase subunit 9 into the DsRed2-N1 vector plasmid. DNA encoding truncated human Bid inserted into the pUC-CAGGS expression vector (27) and DNAs encoding rat Fzo1A/B inserted into the pCMV14 expression vector (Sigma) were also used. Cells (1×10^6) were transfected with plasmid DNA using the Amaxa electroporation system according to the supplier's protocol (kit V, program U-20). The efficiency of transfection was more than 75% as assessed by cotransfection of Su9-DsRed2 DNA. All the siRNAs used were produced by Dharmacon Research, and the sequences were as follows (numbers in parentheses indicate nucleotide positions within the respective open reading frame): rat Fzo1A-siRNA (46–66), 5′-AAGGACAAGCGACAC-AUGGCU-3′; rat Fzo1B-siRNA (110–130), 5′-AAGCAACAUACAGGA-ACCCGG-3′; rat Dnm1-siRNA (96–116), 5′-AACUCAGAGCAGUGGA-AAGAG-3′; human Mfn1-siRNA (46–66), 5′-AAGGGGAUUACUGCA-AUCUUU-3′; human Mfn2-siRNA (52–72) 5′-AAGAGACACAUGGCU-GAGGUG-3′; human Drp1-siRNA (96–116) 5′-AACGCAGAGCAGCG-GAAAGAG-3′; and GFP-siRNA (274–294), and 5′- GGCUACGUCCA-GGAGCGCACC-3′. Cells (Rat1 or HeLa cells) were transfected twice on alternate days with 10 μg of siRNA using the Amaxa electroporation system.

Analysis of Mitochondrial Morphology and Immunocytochemistry—HeLa cells, Rat1 cells, and MEFs were transiently transfected with Su9-DsRed2, and mitochondrial morphology was analyzed under a fluorescence microscope (Zeiss; LSM510META). To determine the localization of Drp1, HeLa cells were grown in 8-well chamber slides and then fixed in 4% paraformaldehyde for 20 min at room temperature, permeabilized with 0.1% Triton X-100 for 20 min at room temperature, and blocked with 2% bovine serum albumin in PBS for 30 min at room temperature. Next, the cells were incubated with anti-Drp1 monoclonal antibody for 1 h at room temperature. After washing with PBS, the cells were stained with goat anti-mouse Alexa Fluor 488 antibody, washed twice with PBS, and examined under a confocal microscope.

Subcellular Fractionation—To assess Bax translocation and cytochrome *c* release, subcellular fractionation was performed using digitonin, as described previously (28). Briefly, after washing twice with PBS, cells were suspended in buffer (20 mM potassium HEPES, pH 7.4, 10 mM KCl, 1.5 mM $MgCl_2$, 250 mM sucrose, 0.1 μM phenylmethylsulfonyl fluoride, and 1 mM dithiothreitol), and treated with 30 μg/ml digitonin for 5 min at 37 °C. Centrifugation was used to separate the cytosolic and organellar fractions, followed by lysis with radioimmune precipitation assay buffer (50 mM Tris-HCl, pH 7.5, 150 mM NaCl, 1% Nonidet P-40, 0.5% deoxycholate, and 0.1% SDS). Isolation of the heavy membrane fraction enriched in mitochondria for measurement of Drp1 was done as described previously (29). Finally, aliquots of each fraction were subjected to Western blot analysis.

Analysis of Protein Oligomerization—Oligomerization of Bak was investigated by gel filtration chromatography. HeLa cells were harvested, washed twice with PBS, and lysed with HNC buffer (25 mM sodium HEPES, pH 7.5, 300 mM NaCl, 2% CHAPS, 1 mM dithiothreitol, and 0.1 μM phenylmethylsulfonyl fluoride). After sonication and centrifugation (15,000 rpm for 15 min), the cell extract was collected and loaded onto a Superdex 200 HR 10/30 column (Amersham Biosciences) equilibrated in HNC buffer without dithiothreitol. Fractions of 96 μl were collected, and aliquots of each fraction were subjected to Western blotting.

To detect oligomerization of Bax, HeLa cells were treated with etoposide, harvested, and washed twice with PBS. Then the cells were resuspended in PBS, and Me_2SO (control) or bismaleimidohexane was added at a final concentration of 0.1 mM. After incubation for 30 min at room temperature, the cells were collected and resuspended in protein sample buffer containing dithiothreitol to quench the cross-linking reaction.

Analysis of Cell Death—HeLa cells and Rat1 cells were treated with 200 μM etoposide or 1 μg/ml anti-human Fas antibody (CH-11). Apoptotic cells were detected by examination of nuclear morphology after staining with Hoechst 33342 (1 μM).

Permeabilized Cells—HeLa cells grown in 10-well poly-L-lysine-coated glass slides, washed twice with isotonic buffer (20 mM potassium HEPES, pH 7.4, 1.5 mM $MgCl_2$, 10 mM KCl, 250 mM sucrose), permeabilized with 20 μg/ml digitonin for about 4 min at room temperature, and then washed with isotonic buffer. Permeabilized cells were incubated with recombinant human Bid protein for 10 min at 37 °C, washed with isotonic buffer, and fixed with 4% paraformaldehyde. Then the fixed cells were stained with anti-Bak (Ab-1) or anti-cytochrome *c* antibodies for 1 h at room temperature.

RESULTS

Apoptotic Mitochondrial Fragmentation and Translocation of Drp1 Are Bcl-2-independent Processes—Recent studies have shown that fragmentation of the mitochondrial network occurs during an early stage of apoptosis (21, 29, 30). To confirm this, HeLa cells were transiently transfected with DNA encoding mitochondria-targeting DsRed2 and then treated with etoposide (an inhibitor of topoisomerase II). By transfection of cells with this plasmid, the mitochondria were specifically stained red irrespective of their membrane potential (data not shown). Whereas many mitochondria were elongated and created a network in healthy cells, the mitochondria became fragmented after addition of etoposide (Fig. 1, *A* and *B*), confirming previous observations (21, 29, 30). This change occurred at an early stage of apoptosis and was not affected by the caspase(s) inhibitor z-VAD-fmk or by Bcl-2 overexpression (Fig. 1, *A* and *B*), both of which almost completely inhibited apoptosis (Fig. 1*B*), suggesting that apoptotic mitochondrial fragmentation is a Bcl-2-insensitive and caspase-independent process. Apoptotic mitochondrial fragmentation was also observed when cells were subjected to other stimuli, such as anti-Fas and staurosporine, and also when other cell lines (COS7 and Rat1) were tested (data not shown). However, mouse embryonic fibroblast cells (MEFs) showed very limited mitochondrial fragmentation during etoposide-induced apoptosis (Fig. 1*C*).

To examine whether the mitochondrial fission machinery was involved in apoptotic mitochondrial fragmentation, we examined the localization of a mitochondrial fission protein Drp1, which has been reported to accumulate in the mitochondria during fission as well as apoptosis in some cell lines (21, 30). Subcellular fractionation analysis revealed that etoposide induced translocation of a significant amount (approximately one-fifth) of Drp1 to the mitochondria (Fig. 1*D*). This was also confirmed by immunofluorescence study: after the cells were treated with etoposide, colocalization of Drp1 with Su9-DsRed2 increased as judged by significant increase of *yellow color* in the *merged photos* (Fig. 1*E*). Although etoposide-treated MEFs

[1] The abbreviations used are: z-VAD-fmk, benzyloxycarbonyl-VAD-fluoromethyl ketone; MEF, mouse embryonic fibroblast; siRNA, small interference RNA; PBS, phosphate-buffered saline; CHAPS, 3-[(3-cholamidopropyl)dimethylammonio]-1-propanesulfonic acid; GAPDH, glyceraldehyde-3-phosphate dehydrogenase.

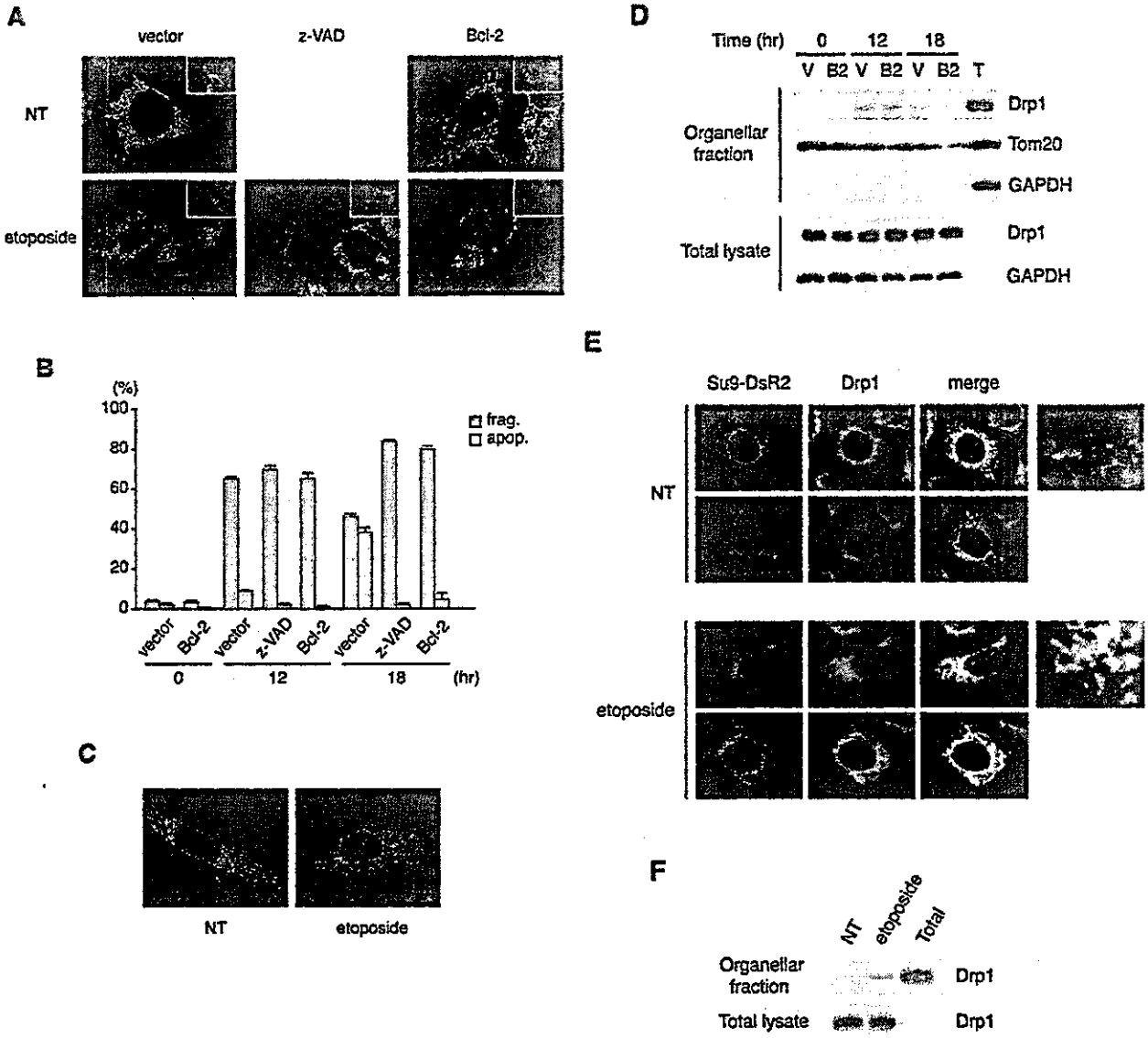

FIG. 1. **Induction of mitochondrial fragmentation and translocation of Drp1 at an early stage of apoptosis in a Bcl-2-independent manner.** *A* and *B*, no effect of Bcl-2 and z-VAD-fmk on etoposide-induced mitochondrial fragmentation. HeLa cells and HeLa cells overexpressing human Bcl-2 were transfected with DNA encoding Su9-DsRed2 (0.05 μg) and were treated with 200 μM etoposide for 16 h (*A*) or for the indicated times (*B*) in the presence or absence of z-VAD-fmk (100 μM). Mitochondrial morphology was observed under a confocal fluorescence microscope. *A*, representative images are shown. Magnified views (*frag.*) are shown in *insets*. *B*, cells with fragmented mitochondria were counted under a confocal microscope. A punctiform mitochondrial phenotype was defined as a loss of the majority of the tubular mitochondria. Apoptotic cells were counted by examination of nuclear morphology after staining with Hoechst 33342. The mean ± S.D. of three independent experiments is shown. *C*, etoposide-induced mitochondrial fragmentation in MEFs. MEFs were transfected with Su9-DsRed2 DNA (0.05 μg) and were treated with 10 μM etoposide for 16 h in the presence of z-VAD-fmk (100 μM). Then mitochondrial morphology was observed using a confocal fluorescence microscope. Representative images are shown. *D*, no effect of Bcl-2 on translocation of Drp1 during apoptosis. HeLa cells (*V*) and HeLa cells overexpressing human Bcl-2 (*B2*) were treated with etoposide. At the indicated times, the mitochondrial fraction was isolated and translocation of Drp1 was evaluated by Western blotting. Tom20 and GAPDH were monitored to verify successful fractionation and equal loading. "*T*" represents the same amount of total lysate. *E*, accumulation of Drp1 to the mitochondria after etoposide treatment. HeLa cells were transfected with DNA encoding Su9-DsRed2 and were treated with 200 μM etoposide. After 16 h, the cells were fixed and stained with anti-Drp1 (*green*) antibody. *F*, etoposide-induced translocation of Drp1 to the mitochondria in MEFs. Cells were transfected with Su9-DsRed2 DNA (0.05 μg) and treated with 10 μM etoposide for 16 h in the presence of z-VAD-fmk (100 μM). Then the mitochondrial fraction was isolated and translocation of Drp1 was evaluated by Western blotting.

showed little apoptotic mitochondrial fragmentation (Fig. 1*C*), there was significant translocation of Drp1 to the mitochondria as in HeLa cells (Fig. 1*F*). These results suggested that mitochondrial fragmentation varies between cell lines while a similar extent of Drp1 translocation to the mitochondria occurs during apoptosis, suggesting possible involvement of Drp1 and the mitochondrial fission apparatus in apoptotic events. Using this method, we also examined whether or not Bcl-2 had an influence on apoptotic translocation of Drp1. As shown in Fig. 1*D*, etoposide induced translocation of Drp1 that was not inhibited by Bcl-2, consistent with the lack of inhibition of apoptotic mitochondrial fragmentation (Fig. 1*A*), indicating that apoptotic translocation of Drp1 to the mitochondria occurs in a Bcl-2-independent manner.

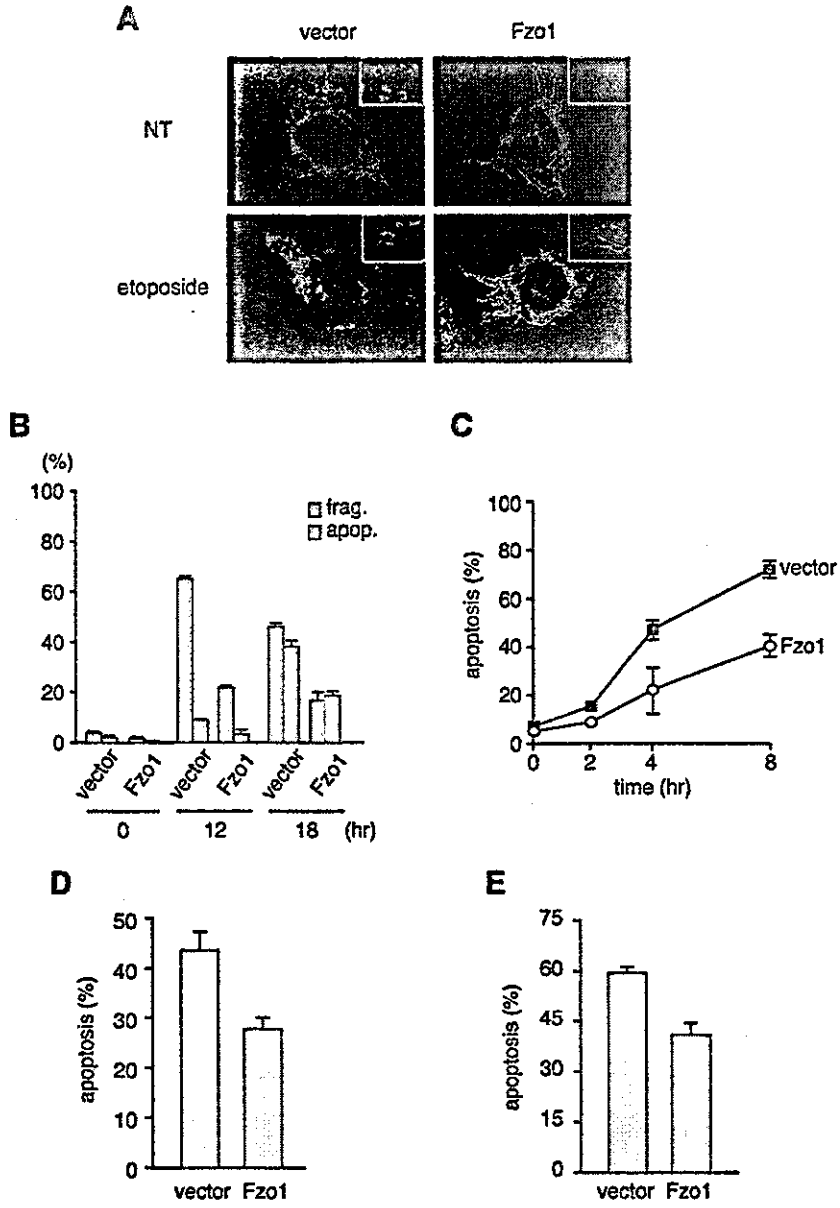

FIG. 2. **Inhibition of mitochondrial fragmentation and apoptosis by Fzo1.** *A* and *B*, inhibition of etoposide-induced mitochondrial fragmentation by Fzo1. HeLa cells were transfected with Su9-DsRed2 DNA (0.05 μg) plus 0.1 μg of empty vector or Fzo1A/B, and then were treated with 200 μM etoposide for 16 h (*A*) or for the indicated times (*B*). Mitochondrial morphology was observed using a confocal fluorescence microscope. *A*, representative images are shown. Magnified views are shown in *insets*. *B*, cells with fragmented mitochondria were counted under a confocal microscope. Then apoptotic cells were counted by examination of nuclear morphology after staining with Hoechst 33342. Data are shown as the mean ± S.D. (n = 3). *C*, inhibition of Fas-induced apoptosis by Fzo1 in HeLa cells. HeLa cells were transfected with 0.1 μg of empty vector or Fzo1A/B for 24 h and then were treated with 1 μg/ml anti-Fas antibody. At the indicated times, the cells were stained with Hoechst 33342, and apoptotic cells were counted under a fluorescent microscope. Values are the mean ± S.D. (n = 3). *D*, inhibition of etoposide-induced apoptosis by Fzo1 in Rat1 cells. Rat1 cells were transfected with 0.1 μg of empty vector or Fzo1A/B and then were treated with 200 μM etoposide. After 20 h, the cells were stained with Hoechst 33342, and apoptotic cells were counted under a fluorescent microscope. Values are the mean ± S.D. (n = 3). *E*, inhibition of etoposide-induced apoptosis by Fzo1 in MEFs. Cells were transfected with 0.3 μg of empty vector or Fzo1A/B and then were treated with 10 μM etoposide. After 16 h, the cells were stained with Hoechst 33342, and apoptotic cells were counted under a fluorescent microscope. Values are the mean ± S.D. (n = 3).

Fzo1 Inhibits Etoposide-induced Apoptotic Mitochondrial Fragmentation and Various Types of Apoptosis—We next examined whether apoptosis was influenced by the inhibition of mitochondrial fission. Rat Fzo1 (corresponding to human Mfn), an essential protein for mitochondrial fusion, was introduced into HeLa cells. Because rats have two *Fzo1* genes (*Fzo1A* and *Fzo1B*) that show 60% amino acid identity and are both essential for mitochondrial fusion (19), we introduced these two genes into HeLa cells concomitantly. Overexpression of Fzo1A/B increased elongated mitochondria (Fig. 2*A*). Not only etoposide-induced mitochondrial fragmentation, but also etoposide-induced apoptosis, was markedly delayed by Fzo1 overexpression (Fig. 2, *A* and *B*). Similar results were obtained when HeLa cells were treated with anti-Fas antibody (Fig. 2*C*), when Rat1 cells were treated with etoposide (Fig. 2*D*), and when MEFs were treated with etoposide (Fig. 2*E*). These results indicated that Fzo1A/B delays various types of apoptosis, possibly by inhibiting apoptotic mitochondrial fission.

Silencing of Fzo1 and Dnm1 (Proteins Involved in Mitochondrial Fusion and Fission) Alters Sensitivity of Cells to Apoptotic Stimuli—To determine whether alterations in the expression of genes involved in mitochondrial fusion/fission could influence the sensitivity of cells to apoptosis, we tested the effect of silencing rat Fzo1A/B and Dnm1 (a protein involved in fission) in Rat1 cells. As shown in Fig. 3*A*, Fzo1 and Dnm1 were almost completely eliminated by 48 h after the introduction of siRNA. After silencing of Fzo1, the filamentous mitochondrial network disappeared (Fig. 3*B*, *middle panel*), whereas silencing of Dnm1 resulted in the formation of elongated and interconnected mitochondria (Fig. 3*B*, *right panel*). When the cells were subsequently treated with etoposide, Fzo1-silenced cells were more sensitive to apoptosis than control cells, whereas Dnm1-silenced cells were more resistant to apoptosis (Fig. 3*C*). Similar results were obtained when HeLa cells were subjected to silencing of Mfn1/2 (the human homologs of Fzo1B/A, respectively) or Drp1 (the human homolog of Dnm1) (Fig. 3, *D* and *E*). Although cells with silencing of Fzo1A/B or Mfn1/2 showed

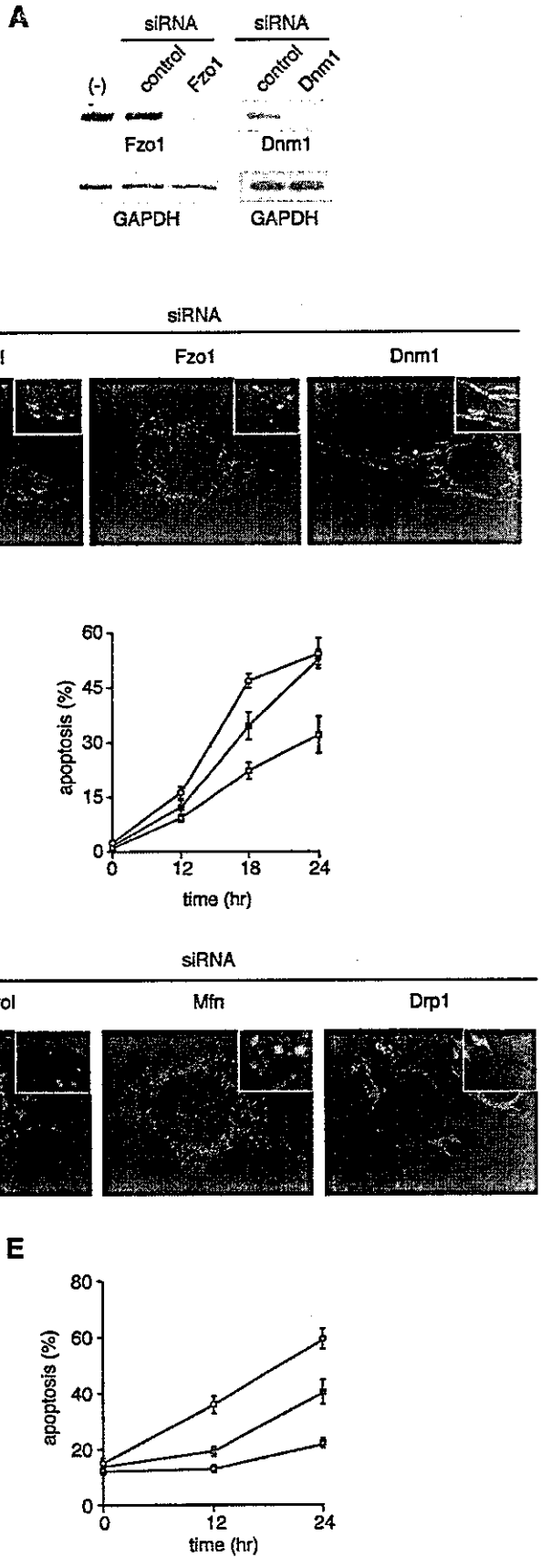

FIG. 3. **Mitochondrial fusion/fission balance affects sensitivity of cells to apoptotic stimuli.** *A–C*, the effect of silencing of Fzo1 or Dnm1 on mitochondrial morphology and apoptosis of Rat1 cells. Rat1 cells were transfected twice on alternate days with either GFP siRNA, Fzo1A/B siRNA, or Dnm1 siRNA. *A*, at 48 h after the second transfection with siRNAs, expression of Fzo1A/B, Dnm1, and GAPDH (as a control) was analyzed by Western blotting. *B*, cells were treated as in *A*, and mitochondrial morphology (detection of Su9-DsRed2) was observed using a confocal fluorescence microscope. Representative images are shown. Magnified views are shown in *insets*. *C*, at 48 h after the second transfection, cells were treated with etoposide (200 μM). At the indicated times, apoptotic cells were counted by examining nuclear morphology. *Closed squares*: GFP siRNA; *open circles*: Fzo1A/B siRNA; *open squares*: Dnm1 siRNA. Data are shown as the mean ± S.D. (n = 3). *D* and *E*, the effect of silencing Mfn1/2 or Drp1 on mitochondrial morphology and apoptosis in HeLa cells. The same experiments as in *B* and *C* were performed using HeLa cells with either GFP siRNA, Mfn1/2 siRNA, or Drp1 siRNA. *Closed squares*: GFP siRNA; *open circles*: Mfn1/2 siRNA; *open squares*: Drp1 siRNA. Data are shown as the mean ± S.D. (n = 3).

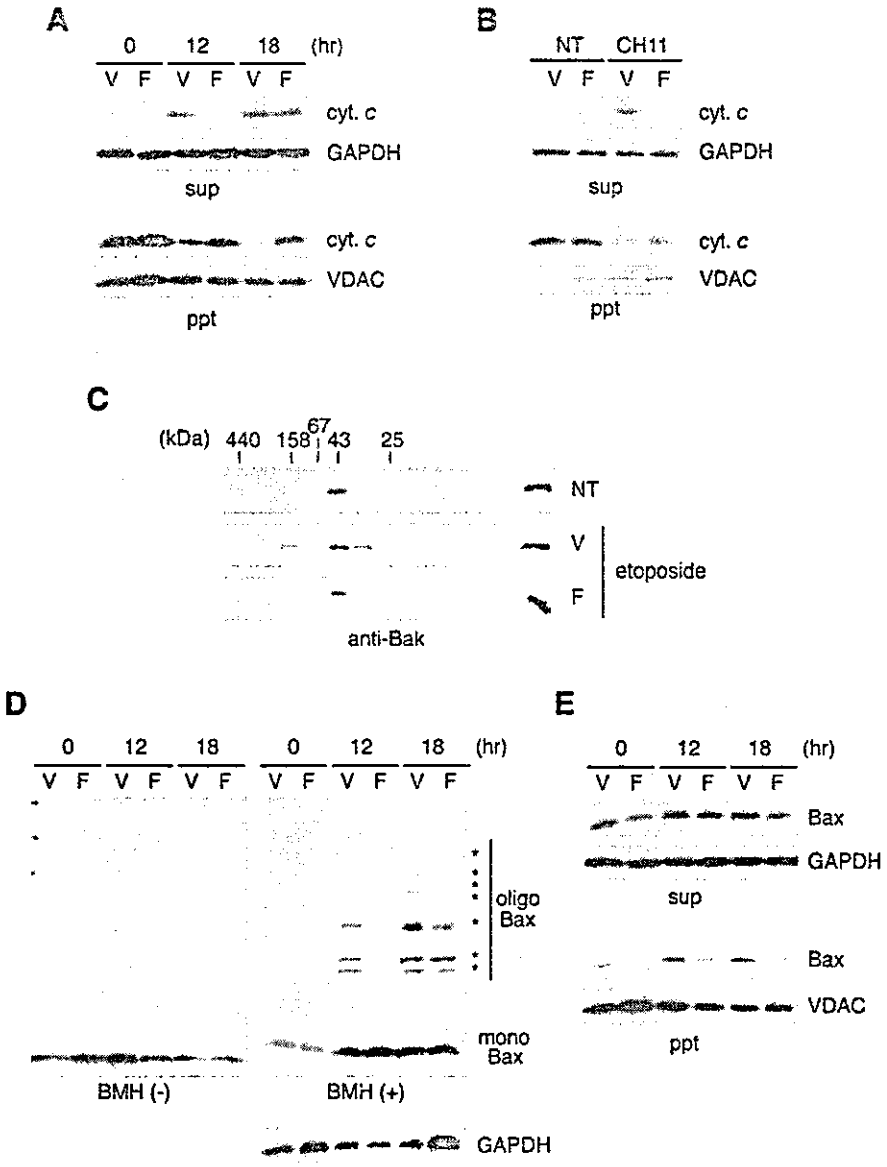

FIG. 4. **Fzo1 delays apoptosis by inhibiting Bax/Bak activation and cytochrome *c* release.** *A* and *B*, inhibition of cytochrome *c* release by Fzo1. HeLa cells were transfected with 0.1 μg of empty vector (*V*) or Fzo1A/B (*F*) and then treated with 200 μM etoposide (*A*) or 1 μg/ml anti-Fas antibody (*B*), followed by subcellular fractionation at the indicated times (*A*) or at 4 h (*B*) as described under "Experimental Procedures." The organellar (*ppt*) and cytosolic fractions (*sup*) were analyzed by Western blotting with anti-cytochrome *c*, anti-VDAC (organellar marker), and anti-GAPDH (cytosolic marker) antibodies. *C* and *D*, inhibition of etoposide-induced Bax and Bak oligomerization by Fzo1. HeLa cells were transfected with 0.1 μg of empty vector (*V*) or Fzo1A/B (*F*) and then were treated with 200 μM etoposide. *C*, after 12 h, the cells were lysed by sonication in HNC buffer and centrifuged, and the supernatants were subjected to gel filtration analysis. Aliquots of each fraction were subjected to Western blotting using anti-Bak antibody. *D*, at the indicated times, cells were incubated with Me_2SO or with 0.1 mM bismaleimidohexane. Bax oligomers (*) were detected by Western blotting using an anti-Bax (N-20) antibody. *E*, inhibition of etoposide-induced Bax translocation by Fzo1. The same experiment as shown in *A* was performed, and Bax was analyzed by Western blotting.

fragmented mitochondria, death did not occur without apoptotic stimulation (Fig. 3, *C* and *E*). All these results indicated that modulation of genes involved in mitochondrial fusion and fission could significantly influence the sensitivity of cells to apoptosis.

Fzo1 Inhibits Etoposide-induced Apoptosis by Delaying Cytochrome c Release and Bax/Bak Activation—How does Fzo1 inhibit apoptosis? Bax and Bak, which act as a gateway for various apoptotic signals at the mitochondria, are thought to exist as inactive forms in healthy cells, and various apoptotic stimuli may cause their activation through conformation changes and oligomerization, leading to cytochrome *c* release from the mitochondria (5, 6). Therefore, we first examined the effect of Fzo1 on apoptotic cytochrome *c* release in HeLa cells. As shown in Fig. 4 (*A* and *B*), Fzo1 delayed etoposide-induced and Fas-mediated release of cytochrome *c*, indicating that Fzo1 acted upstream of cytochrome *c* release. Next, we examined the effect of Fzo1 on etoposide-induced activation of Bax/Bak and found that oligomerization of both Bax and Bak was markedly delayed by Fzo1 expression (Fig. 4, *C* and *D*). Bax (but not Bak) is mainly localized in the cytoplasm of healthy cells and shows translocation to the mitochondria after apoptotic stimulation. Interestingly, overexpression of Fzo1 inhibited apoptotic mitochondrial localization of Bax (Fig. 4*E*), which might have led to

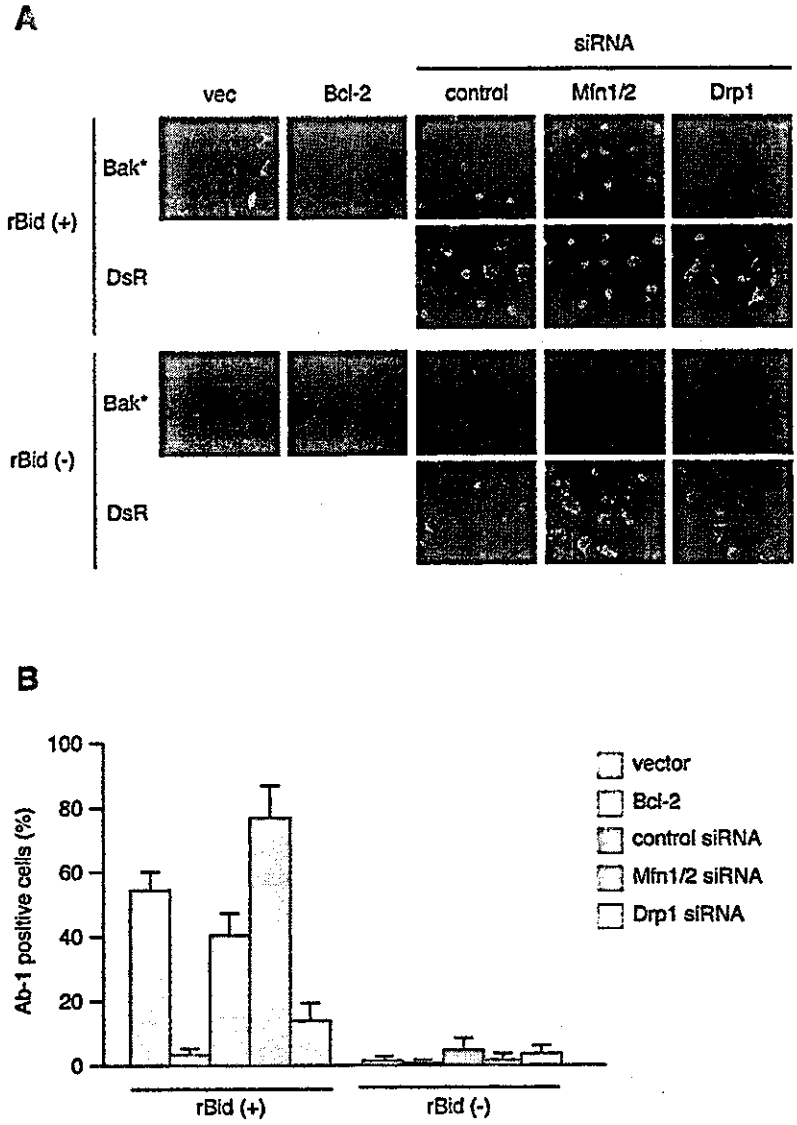

FIG. 5. **Mitochondrial fusion/fission balance affects mitochondrial sensitivity to recombinant Bid.** HeLa cells were transfected twice on alternate days with the indicated siRNAs together with Su9-DsRed2 DNA. At 48 h after the second transfection, cells were permeabilized with digitonin and then incubated with recombinant human Bid (1 μg) for 10 min at 37 °C. Next, the cells were fixed and immunostained using a conformation-specific Bak monoclonal antibody (Ab-1) that only bound to activated Bak (*A* and *B*), or an anti-cytochrome *c* monoclonal antibody (*C* and *D*). Bcl-2-overexpressing HeLa cells were used as a control. Note that cells with cytochrome *c* release did not show a cytochrome *c* signal (*arrows*) due to leakage through the permeabilized plasma membrane. *A* and *C*, representative images are shown. *B* and *D*, Ab1-positive cells (*B*) and cells with cytochrome *c* release (*D*) were counted in three randomly chosen fields under a confocal microscope. Data are shown as the mean ± S.D. (n = 3).

a delay in Bax activation. Taken together, these findings indicate that Fzo1 expression delayed the activation of Bax/Bak and thereby inhibited both cytochrome *c* release and apoptosis.

The Balance between Fusion and Fission Proteins Affects Mitochondrial Sensitivity to Death Stimuli—Changes in the levels of proteins involved in mitochondrial fusion/fission had an effect on apoptosis. Overexpression of Fzo1 inhibited apoptotic mitochondrial fragmentation and delayed Bax/Bak activation and cytochrome *c* release during apoptosis, raising the possibility that changes of the proteins involved in mitochondrial fusion/fission could alter mitochondrial sensitivity to apoptotic stimulation. To examine this issue, HeLa cells were transfected with siRNA for Mfn1/2 or Drp1, permeabilized with digitonin, and then incubated with recombinant Bid, which is a pro-apoptotic member of the Bcl-2 family and activates Bax/Bak (5, 6). Using this method, mitochondria in different states could be subjected to the same apoptotic stimulus, and the response was assessed by measuring cytochrome *c* release and Bak activation using a conformation-specific monoclonal antibody that only reacted activated Bak. Immunofluorescence microscopy demonstrated that recombinant Bid caused the activation of Bak in control cells but not in Bcl-2-overexpressing cells (Fig. 5, *A* and *B*). Because activation of Bak is cancelled by Bcl-2 in several cell lines, our *in vitro* system corresponded well with the cellular response. As shown in Fig. 5 (*A* and *B*), Mfn1/2-silenced cells largely had fragmented mitochondria and showed enhanced activation of Bak, whereas Drp1-silenced cells had elongated mitochondria and showed resistance to Bak activation. Consistent with these findings, Bid-induced cytochrome *c* release was accelerated by the silencing of Mfn1/2, whereas it was inhibited by silencing of Drp1 (Fig. 5, *C* and *D*). All these results suggested that the balance between mitochondrial fusion/fission proteins could affect mitochondrial sensitivity to apoptotic stimuli.

DISCUSSION

Here we showed that 1) mitochondrial fragmentation occurred during apoptosis and was accompanied by mitochondrial translocation of Drp1, whereas 2) changes in levels of mitochondrial fusion/fission proteins (Fzo1 (Mfn) and Dnm1 (Drp1)) affected the sensitivity of the mitochondria and cells to apoptotic stimulation. A higher fusion/fission protein ratio increased the resistance of mitochondria and cells to apoptotic stimulation, whereas a lower ratio had the opposite effect.

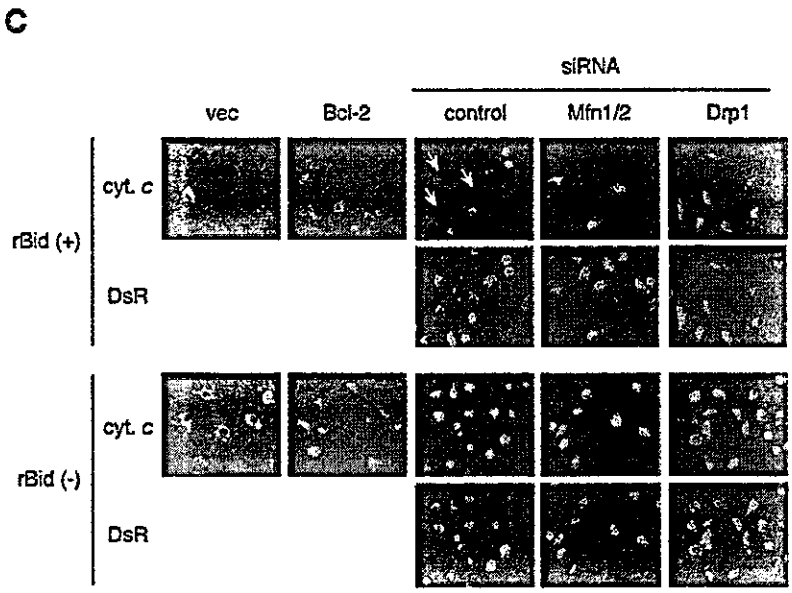

FIG. 5—*continued*

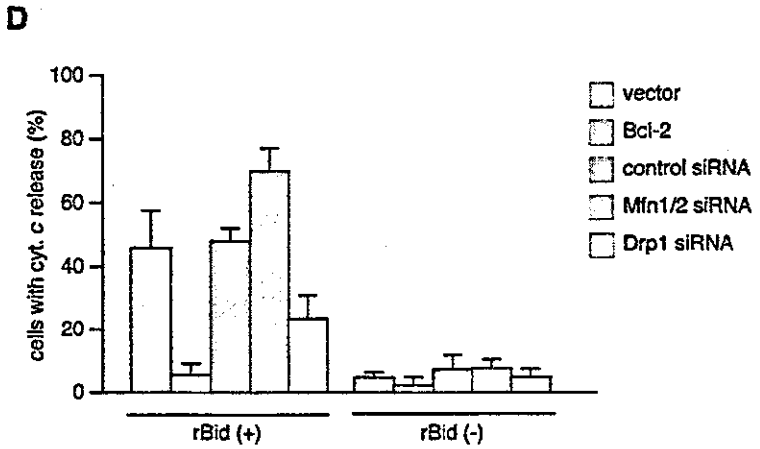

Because mitochondrial fragmentation was not observed in some cell lines, this process does not seem to be a prerequisite for apoptosis but rather to contribute to increased sensitivity to apoptotic stimuli.

How does the mitochondrial fusion/fission protein balance affect apoptosis? Although detailed mechanisms remain to be elucidated, one possibility is that, because fission and fusion of phospholipid membranes are regulated by these proteins, the mitochondrial lipid composition changes when the balance between fusion and fission protein is altered. Accumulating evidence indicates that changes of the phospholipid composition of the mitochondrial membrane can influence apoptosis. It has been reported that cardiolipin, which is a unique phospholipid in the mitochondria, is essential for the functioning of tBid during apoptosis (31) and for Bax-mediated permeabilization of liposomes (32), and that the intramitochondrial distribution of cardiolipin alters during apoptosis (33). Cardiolipin is localized in the inner mitochondrial membrane and accumulates at intermembrane contact sites (34), which have been suggested as a target for tBid and Bax (35, 36). Changes in the levels of mitochondrial fusion/fission proteins might alter the cardiolipin content of the mitochondrial membrane, thus affecting the sensitivity of the mitochondria and cells to apoptotic stimulation.

We also showed that Mfn/Fzo1-silenced cells, in which the mitochondria underwent fragmentation, did not die in the absence of additional apoptotic stimuli. These results were inconsistent with previous reports suggesting that silencing of Opa1 or overexpression of Fis1 caused both mitochondrial fragmentation and apoptosis (24, 25), so it is possible that Fis1 expression or Opa1 silencing not only provides a fission signal but also an apoptotic signal.

We also confirmed the previous observations (21, 29, 30) that Drp1 translocates from the cytosol to the mitochondria during apoptosis, although the mechanism regulating Drp1 translocation is unknown. It has been reported that a dominant negative mutant of Drp1 suppresses some forms of apoptosis (21), suggesting that the translocation of Drp1 to the mitochondria might be important for apoptosis by triggering mitochondrial fragmentation. We found that overexpression of Fzo1 significantly delayed the mitochondrial translocation of Drp1 (data not shown).

In this study, Bcl-2 did not inhibit either apoptotic mitochondrial fragmentation or translocation of Drp1 to the mitochondria (Fig. 1). We also found that apoptosis-induced transloca-

tion of Drp1 occurs equally in the absence of Bax and Bak (data not shown). Consistently, apoptotic mitochondrial fragmentation and Drp1 translocation were not observed when apoptosis was induced by overexpression of truncated Bid (tBid) (data not shown). Taken together, these results suggest that the Bcl-2 family of proteins does not seem to be involved in the processes of apoptotic mitochondrial fragmentation and Drp1 translocation, suggesting that various apoptotic stimuli (including etoposide, anti-Fas, etc.) not only activate Bax/Bak but also promote mitochondrial fragmentation that sensitizes the mitochondria to apoptotic signals.

Finally, it is interesting to note that several diseases are associated with mutations of genes involved in mitochondrial fusion/fission. Mutations of the *opa1* gene have been reported in autosomal dominant optic atrophy patients with degeneration of the retinal ganglion cells (37). Furthermore, it has been described that a mutation of the *mfn2* gene causes Charcot-Marie-Tooth neuropathy type 2A (38). It is possible that defects of mitochondrial fusion/fission might alter the susceptibility of cells to apoptotic death and, thus, cause these diseases.

Acknowledgments—We are grateful to Drs. N. Ishihara and K. Mihara (Graduate School of Medical Science, Kyushu University) for providing rat Fzo1A/B cDNAs and for helpful discussion.

REFERENCES

1. Wang, X. (2001) *Genes Dev.* **15,** 2922–2933
2. Green, D. R. (2000) *Cell* **102,** 1–4
3. Martinou, J. C., and Green, D. R. (2001) *Nat. Rev. Mol. Cell. Biol.* **2,** 63–67
4. Zamzami, N., and Kroemer, G. (2001) *Nat. Rev. Mol. Cell. Biol.* **2,** 67–71
5. Tsujimoto, Y. (2003) *J. Cell. Physiol.* **195,** 158–167
6. Danial, N. N., and Korsmeyer, S. J. (2004) *Cell* **116,** 205–219
7. Malisan, F., and Testi, R. (2003) *Curr. Med. Chem.* **10,** 1573–1580
8. Bleazard, W., McCaffery, J. M., King, E. J., Bale, S., Mozdy, A., Tieu, Q., Nunnari, J., and Shaw, J. M. (1999) *Nat. Cell Biol.* **1,** 298–304
9. Mozdy, A. D., McCaffery, J. M., and Shaw, J. M. (2000) *J. Cell Biol.* **151,** 367–380
10. Tieu, Q., and Nunnari, J. (2000) *J. Cell Biol.* **151,** 353–366
11. Messerschmitt, M., Jakobs, S., Vogel, F., Fritz, S., Dimmer, K. S., Neupert, W., and Westermann, B. (2003) *J. Cell Biol.* **160,** 553–564
12. Labrousse, A. M., Zappaterra, M. D., Rube, D. A., and van der Bliek, A. M. (1999) *Mol. Cell* **4,** 815–826
13. Smirnova, E., Shurland, D. L., Ryazantsev, S. N., and van der Bliek, A. M. (1998) *J. Cell Biol.* **143,** 351–358
14. Rapaport, D., Brunner, M., Neupert, W., and Westermann, B. (1998) *J. Biol. Chem.* **273,** 20150–20155
15. Hermann, G. J., Thatcher, J. W., Mills, J. P., Hales, K. G., Fuller, M. T., Nunnari, J., and Shaw, J. M. (1998) *J. Cell Biol.* **143,** 359–373
16. Sesaki, H., and Jensen, R. E. (2001) *J. Cell Biol.* **152,** 1123–1134
17. Wong, E. D., Wagner, J. A., Gorsich, S. W., McCaffery, J. M., Shaw, J. M., and Nunnari, J. (2000) *J. Cell Biol.* **151,** 341–352
18. Hales, K. G., and Fuller, M. T. (1997) *Cell* **90,** 121–129
19. Ishihara, N., Jofuku, A., Eura, Y., and Mihara, K. (2003) *Biochem. Biophys. Res. Commun.* **301,** 891–898
20. Santel, A., and Fuller, M. T. (2001) *J. Cell Sci.* **114,** 867–874
21. Frank, S., Gaume, B., Bergmann-Leitner, E. S., Leitner, W. W., Robert, E. G., Catez, F., Smith, C. L., and Youle, R. J. (2001) *Dev. Cell* **1,** 515–525
22. Karbowski, M., and Youle, R. J. (2003) *Cell Death Differ.* **10,** 870–880
23. Bossy-Wetzel, E., Barsoum, M. J., Godzik, A., Schwarzenbacher, R., and Lipton, S. A. (2003) *Curr. Opin. Cell Biol.* **15,** 706–716
24. Olichon, A., Baricault, L., Gas, N., Guillou, E., Valette, A., Belenguer, P., and Lenaers, G. (2003) *J. Biol. Chem.* **278,** 7743–7746
25. James, D. I., Parone, P. A., Mattenberger, Y., and Martinou, J. C. (2003) *J. Biol. Chem.* **278,** 36373–36379
26. Shimizu, S., Eguchi, Y., Kamiike, W., Matsuda, H., and Tsujimoto, Y. (1996) *Oncogene* **12,** 2251–2257
27. Niwa, H., Yamamura, K., and Miyazaki, J. (1991) *Gene (Amst.)* **108,** 193–199
28. Nomura, M., Shimizu, S., Ito, T., Narita, M., Matsuda, H., and Tsujimoto, Y. (1999) *Cancer Res.* **59,** 5542–5548
29. Breckenridge, D. G., Stojanovic, M., Marcellus, R. C., and Shore, G. C. (2003) *J. Cell Biol.* **160,** 1115–1127
30. Karbowski, M., Lee, Y. J., Gaume, B., Jeong, S. Y., Frank, S., Nechushtan, A., Santel, A., Fuller, M., Smith, C. L., and Youle, R. J. (2002) *J. Cell Biol.* **159,** 931–938
31. Lutter, M., Fang, M., Luo, X., Nishijima, M., Xie, X., and Wang, X. (2000) *Nat. Cell Biol.* **2,** 754–761
32. Kuwana, T., Mackey, M. R., Perkins, G., Ellisman, M. H., Latterich, M., Schneiter, R., Green, D. R., and Newmeyer, D. D. (2002) *Cell* **111,** 331–342
33. Garcia Fernandez, M., Troiano, L., Moretti, L., Nasi, M., Pinti, M., Salvioli, S., Dobrucki, J., and Cossarizza, A. (2002) *Cell Growth Differ.* **13,** 449–455
34. Schlame, M., Rua, D., and Greenberg, M. L. (2000) *Prog. Lipid Res.* **39,** 257–288
35. Lutter, M., Perkins, G. A., and Wang, X. (2001) *BMC Cell Biol.* **2,** 22
36. Zamzami, N., Brenner, C., Marzo, I., Susin, S. A., and Kroemer, G. (1998) *Oncogene* **16,** 2265–2282
37. Kjer, P., Jensen, O. A., and Klinken, L. (1983) *Acta Ophthalmol. (Copenh.)* **61,** 300–312
38. Zuchner, S., Mersiyanova, I. V., Muglia, M., Bissar-Tadmouri, N., Rochelle, J., Dadali, E. L., Zappia, M., Nelis, E., Patitucci, A., Senderek, J., Parman, Y., Evgrafov, O., Jonghe, P. D., Takahashi, Y., Tsuji, S., Pericak-Vance, M. A., Quattrone, A., Battologlu, E., Polyakov, A. V., Timmerman, V., Schroder, J. M., and Vance, J. M. (2004) *Nat. Genet.* **36,** 449–451

Structures of the Small-Molecule Bcl-2 Inhibitor (BH3I-2) and Its Related Simple Model in Protonated and Deprotonated Forms

Daisuke Kanamori, Taka-aki Okamura, Hitoshi Yamamoto, Shigeomi Shimizu,[1] Yoshihide Tsujimoto,[1] and Norikazu Ueyama*

Department of Macromolecular Science, Graduate School of Science, Osaka University, Toyonaka, Osaka 560-0043

[1]Department of Post-Genomics and Diseases, Graduate School of Medicine, Osaka University, Suita, Osaka 565-0871

Received May 24, 2004; E-mail: ueyama@chem.sci.osaka-u.ac.jp

REPRINTED FROM

Bulletin of the Chemical Society of Japan

Vol.77 No.11 2004 p.2057–2064

November 15, 2004

The Chemical Society of Japan

Structures of the Small-Molecule Bcl-2 Inhibitor (BH3I-2) and Its Related Simple Model in Protonated and Deprotonated Forms

Daisuke Kanamori, Taka-aki Okamura, Hitoshi Yamamoto, Shigeomi Shimizu,[1] Yoshihide Tsujimoto,[1] and Norikazu Ueyama*

Department of Macromolecular Science, Graduate School of Science, Osaka University, Toyonaka, Osaka 560-0043

[1]Department of Post-Genomics and Diseases, Graduate School of Medicine, Osaka University, Suita, Osaka 565-0871

Received May 24, 2004; E-mail: ueyama@chem.sci.osaka-u.ac.jp

3-Bromo-5-chloro-*N*-(2-chlorophenyl)-2-hydroxybenzamide (**BCNCPB–OH**) was synthesized as a model compound of the small-molecule Bcl-2 inhibitor (BH3I-2) and characterized by ^{1}H NMR and IR measurements. The structures of **BCNCPB–OH** and its deprotonated form (**BCNCPB–O–NEt$_4$**) were determined by X-ray analysis. **BCNCPB–OH** has an intramolecular OH···O=C hydrogen bond and **BCNCPB–O–NEt$_4$** has an intramolecular NH···O(oxyanion) hydrogen bond in the solid and solution states. The solution structures of protonated and deprotonated BH3I-2′ (BH3I-2 analogue) were determined by ^{1}H NMR, NOESY, and IR measurements. They have similar conformations to those of the corresponding model compounds. A pK_a value of **BCNCPB–OH** of 5.1 is considered a very low value for phenol derivatives, suggesting the possibility that BH3I-2 binds to protein in the deprotonated form having an intramolecular NH···O(oxyanion) hydrogen bond.

BH3I-2 is a recently identified small-molecule inhibitor of the Bcl-2 family, which is a regulator of apoptotic pathways (Chart 1).[1,2] A number of inhibitors which have a salicylamide skeleton similar to BH3I-2 have been reported to inhibit various enzymes relating to the respiratory chain,[3–6] the biosynthesis of melanin,[7,8] oxidative phosphorylation,[9–11] bacterial two component systems,[12,13] and so on. Although the precise inhibitory mechanisms in many cases are vague, drug development work has indicated that electron-withdrawing substituents[12,13] and hydrophobicity[13] are needed for a high activity. The importance of the salicylamide skeleton and hydrogen bonds on it have been shown by the following evidence. In X-ray structures of the inhibitor–scytalone dehydratase complex[7] and antimycin A_1–cytochrome bc_1 complex (the chemical structure of the inhibitors are depicted in Chart 2),[3,14] hydrogen bonds between amino acid residues in the binding site and phenolic OH, amide NH, and the carbonyl group on the salicylamide moiety were found. In these structures, intramolecular OH···O=C hydrogen bonding on the inhibitor is suggested by a short distance between the phenolic oxygen and carbonyl oxygen. The analogous inhibitor, antimycin A_3, is also represented as an intramolecularly OH···O=C hydrogen-bonded conformation in the proposed structure of antimycin A_3/Bcl-xL (one of the Bcl-2 family proteins) complex.[15,16] Modifications to break intra- and/or intermolecular hydrogen bonds such as the deletion of the phenolic OH or carbonyl group,[8] methylation of the phenolic[17] or amide[4] proton, or the insertion of $-CH_2-$ between the aromatic ring and carbonyl group[4] reduce the inhibitory activity. These results demonstrate that the importance of the salicylamide skeleton arises from its hydrogen bonding ability.

Suezawa et al. has reported that salicylanilide derivatives having a halogen atom (X), a hydrogen bonding acceptor, at the 3-position are in equilibrium between intramolecular

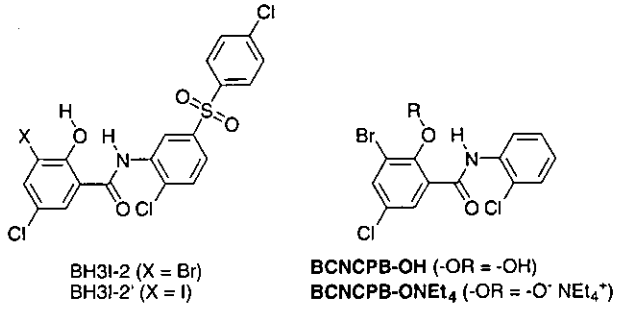

BH3I-2 (X = Br)
BH3I-2′ (X = I)

BCNCPB-OH (-OR = -OH)
BCNCPB-ONEt$_4$ (-OR = -O$^-$ NEt$_4^+$)

Chart 1. Chemical structures of BH3I-2, BH3I-2′, **BCNCPB–OH**, and **BCNCPB–O–NEt$_4$**.

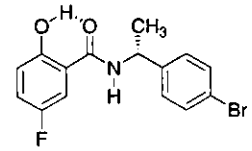

Inhibitor of scytalone dehydratase

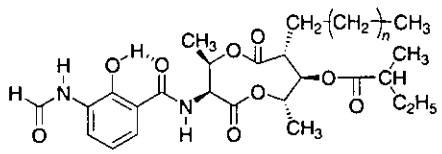

Antimycin A_3 (n = 2), A_1 (n = 4)

Chart 2. Other inhibitors having salicylamide moiety.

Published on the web November 11, 2004; DOI 10.1246/bcsj.77.2057

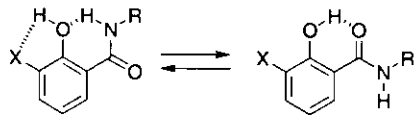

Chart 3. Two hydrogen bonding modes.

NH···O hydrogen bonded (type A) and OH···O=C hydrogen bonded conformations (type B) (Chart 3).[18] Although *O*-acetylation removes the stabilization by the intramolecular OH···O=C hydrogen bond, the type B conformation is major in solution. Salicylanilide derivatives, which can form intramolecular OH···O=C hydrogen bonds, including BH3I-2, probably favor a type B conformation. On the other hand, type A is predominant in deprotonated salicylamide derivatives by intramolecular NH···O(oxyanion) hydrogen bonds.[19,20]

The structure of the BH3I-2/Bcl-xL complex has not been determined by X-ray analysis but computationally proposed using the solution structure of the BakBH3–peptide/Bcl-xL complex.[1,21,22] In this structure, BH3I-2 binds to the hydrophobic cleft formed by BH1, BH2, and BH3 regions and takes a type A conformation depicted in Chart 1. Though it was not discussed in detail whether BH3I-2 is protonated or not, we present here the possibility of the deprotonation. The pK_a values of salicylanilide derivatives have been reported below 7.5, and further lowered by electron-withdrawing substituents.[11] The pK_a value of salicylamide derivatives is also reduced by the NH···O(oxyanion) hydrogen bond in its phenolate anion form.[11,19] Such intramolecular NH···O hydrogen bonds are supported in a hydrophobic environment and efficiently lower the pK_a value, as shown previously in our report for thiophenol (benzenethiol) and benzoic acid analogues.[23,24] In the hydrophobic cleft of Bcl-xL, the pK_a value of BH3I-2 is presumably lowered, and its deprotonated form is stabilized.

In this paper, we determine the structure of BH3I-2 and its deprotonated form and evaluate the pK_a value in a hydrophobic environment using the model compounds discussed below. To realize a hydrophobic environment where BH3I-2 binds, we use organic solvents and a micellar solution.

The determination of the precise hydrogen bonding mode of BH3I-2 in the complex is important because it will be valuable for understanding inhibitory mechanisms in detail. For this purpose, 3-bromo-5-chloro-*N*-(2-chlorophenyl)-2-hydroxybenzamide (**BCNCPB–OH**) and its deprotonated form (**BCNCPB–O–NEt$_4$**) were synthesized and structurally analyzed as model compounds of protonated and deprotonated BH3I-2 (Chart 1), respectively. Because the replacement of the *N*-substituent does not significantly influence inhibitory activity, the 4-chlorophenylsulfonyl group was removed to improve the crystallinity of the BH3I-2 model compounds.[4] The structures and hydrogen bonding modes were determined by X-ray analysis and IR spectra in the solid state and by ^{1}H NMR and IR spectra in solution. The structures of BH3I-2′ (Chart 1) in protonated and deprotonated forms were determined by ^{1}H NMR and IR spectra in solution. The reason BH3I-2′ was employed is that it probably prefers a similar conformation to BH3I-2, which is not available commercially. To evaluate the tendency to deprotonate the phenolic OH, the pK_a value of **BCNCPB–OH** was determined. The pK_a value of BH3I-2 is considered to be comparable to that of **BCNCPB–OH** because introduction of a stronger electron-withdrawing group (NO_2) had a negligible influence on the pK_a value.[11,25]

Results and Discussion

Synthesis. The synthesis of **BCNCPB–OH** and **BCNCPB–O–NEt$_4$** is shown in Scheme 1. The phenolic hydroxy group was protected by an acetyl group to avoid a side reaction. The deprotonation of the phenolic OH was performed by neutralization with NEt_4OH.

Structures of Model Compound in the Protonated and Deprotonated Forms in the Solid State. The molecular structures of protonated (**BCNCPB–OH**) and deprotonated forms (**BCNCPB–O–NEt$_4$**) were determined by X-ray analy-

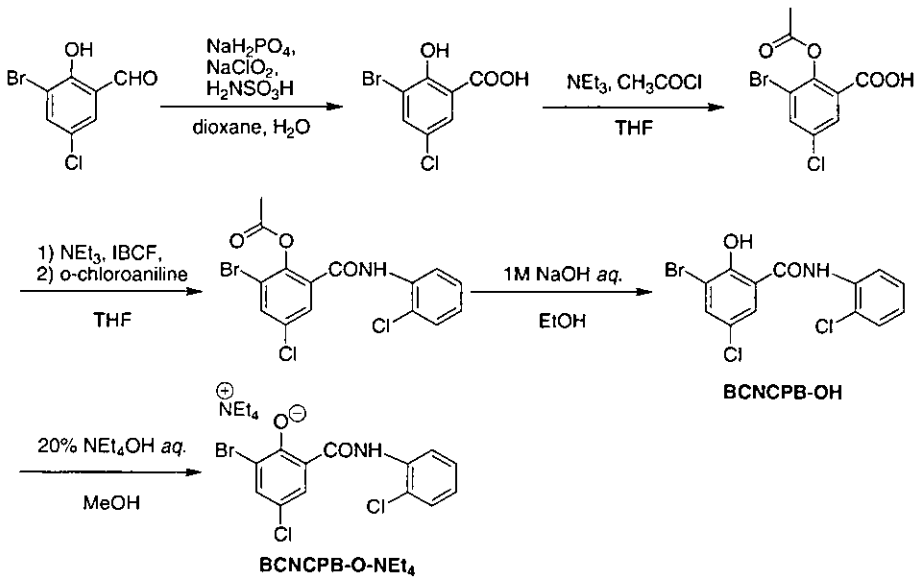

Scheme 1. Synthesis of **BCNCPB–OH** and **BCNCPB–O–NEt$_4$**. IBCF = isobutyl chloroformate.

sis. It has been revealed in the solid state that **BCNCPB–OH** prefers the type B conformation and **BCNCPB–O–NEt$_4$** prefers type A.

The molecular structure of **BCNCPB–OH** is shown in Fig. 1a and the selected short contacts, bond lengths, and torsion angles are listed in Table 1. The presence of an intramolecular OH···O=C hydrogen bond is suggested by the short distances between the phenolic OH proton (H1) and the amide carbonyl oxygen atom (O2) (1.91(3) Å) and between the phenolic oxygen (O1) and O2 (2.606(3) Å). The chlorine atom at the 2′-position in Ar_B (Cl2) is located on the opposite side of the carbonyl group to avoid electrostatic repulsion. The location of the chlorine atom suggests the presence of the attractive interaction between the amide NH proton (H2) and Cl2 (Cl2–H2 is 2.51(2) Å). The coplanarity between the amide plane and two aromatic rings is indicated where the torsion angles are 160.0(3)° (C5–C6–C7–O2) and 176.9(3)° (C7–N1–C8–C9). The presence of an intermolecular OH···O=C hydrogen bond is suggested by the short distance between the phenolic hydrogen atom (H1) and amide carbonyl oxygen atom (O2*) of the neighboring molecule (2.50(3) Å) (Fig. 1b). No significant intermolecular interaction around the amide NH exists.

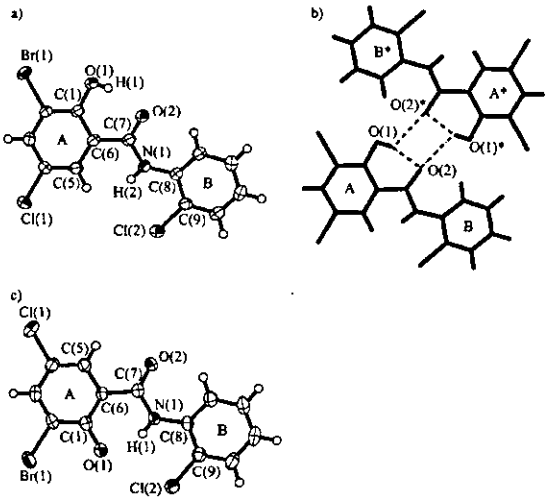

Fig. 1. ORTEP drawing (a) and packing structure (b) of **BCNCPB–OH** and ORTEP drawing of anion part of **BCNCPB–O–NEt$_4$** (c).

The crystal structure of the deprotonated form (**BCNCPB–O–NEt$_4$**) is shown in Fig. 1c. A different hydrogen bonding mode from that in **BCNCPB–OH** was found. The short distances between the phenoxy oxygen (O1) and the amide proton (H1) (1.87(2) Å) and between O1 and the amide nitrogen (N1) (2.583(2) Å) suggest the presence of an intramolecular NH···O(oxyanion) hydrogen bond. The relative orientation of chlorine at the 2′-position in Ar_B (Cl2) toward the amide NH is similar to that in **BCNCPB–OH**. The coplanarity of **BCNCPB–O–NEt$_4$** is higher than in **BCNCPB–OH**. The torsion angle between Ar_A and amide plane (C5–C6–C7–O2) is −1.2(3)°, and that between the amide plane and Ar_B (C7–N1–C8–C9) is −175.6(2)°. The C1–O1 bond length in **BCNCPB–O–NEt$_4$** (1.282(3) Å) is shorter than that in **BCNCPB–OH** (1.340(3) Å) due to an increase in the double bond character of the C1–O1 bond caused by the delocalization of the negative charge of the phenoxy anion to the aryl ring.

The most significant structural change between **BCNCPB–OH** and **BCNCPB–O–NEt$_4$** is a ca. 180 degree rotation about the C6–C7 bond.

The presence of hydrogen bonds in the solid state was confirmed by IR measurements in a Nujol mull (Fig. 2). In the protonated form, **BCNCPB–OH**, an amide NH stretching band was observed at 3416 cm^{-1}, which is slightly lower than non-hydrogen-bonded ν(NH) (ν(NH) of salicylanilide in dilute solution[20] is 3456 cm^{-1}) and comparable to NH···Cl hydrogen-bonded ν(NH).[26,27] The orientation of Cl toward the carbonyl C=O and the amide NH is controlled by not only the electrostatic repulsion between the carbonyl oxygen and Cl but also the NH···Cl hydrogen bond. In **BCNCPB–O–NEt$_4$**, it is

Table 1. Selected Short Contacts, Bond Distance, and Torsion Angles of **BCNCPB–OH** and **BCNCPB–O–NEt$_4$**

BCNCPB–OH		**BCNCPB–O–NEt$_4$**	
	Short contacts/Å		
H(2)···Cl(2)	2.51(2)	H(1)···Cl(2)	2.54(2)
H(1)···O(2)	1.91(3)	H(1)···O(1)	1.87(2)
O(1)···O(2)	2.606(3)	O(1)···N(1)	2.583(2)
H(1)···O(2)*	2.50(3)		
O(1)···O(2)*	2.921(3)		
	Bond lengths/Å		
C(1)–O(1)	1.340(3)	C(1)–O(1)	1.282(3)
O(2)–C(7)	1.223(4)	O(2)–C(7)	1.239(3)
C(6)–C(7)	1.498(4)	C(6)–C(7)	1.484(3)
N(1)–C(7)	1.353(4)	N(1)–C(7)	1.360(3)
N(1)–C(8)	1.402(4)	N(1)–C(8)	1.400(3)
O(1)–H(1)	0.74(3)	N(1)–H(1)	0.80(2)
N(1)–H(2)	0.87(3)		
	Torsion angles/°		
O(2)–C(7)–C(6)–C(5)	−160.0(3)	O(2)–C(7)–C(6)–C(5)	−1.2(3)
C(7)–N(1)–C(8)–C(9)	176.9(3)	C(7)–N(1)–C(8)–C(9)	−175.6(2)

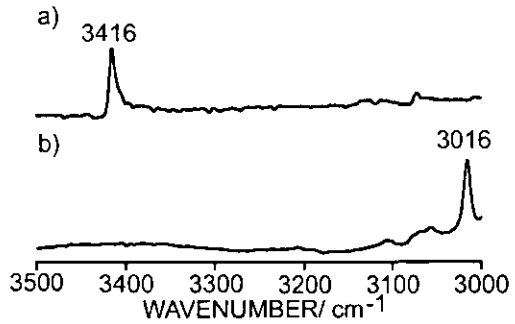

Fig. 2. IR spectra in a Nujol mull of **BCNCPB–OH** (a) and **BCNCPB–O–NEt$_4$** (b).

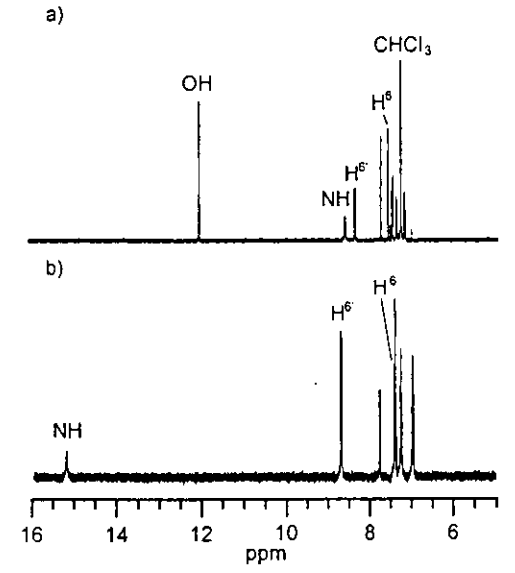

Fig. 3. ^{1}H NMR spectra of **BCNCPB–OH** in $CDCl_3$ (a) and **BCNCPB–O–NEt$_4$** in CD_3CN (b).

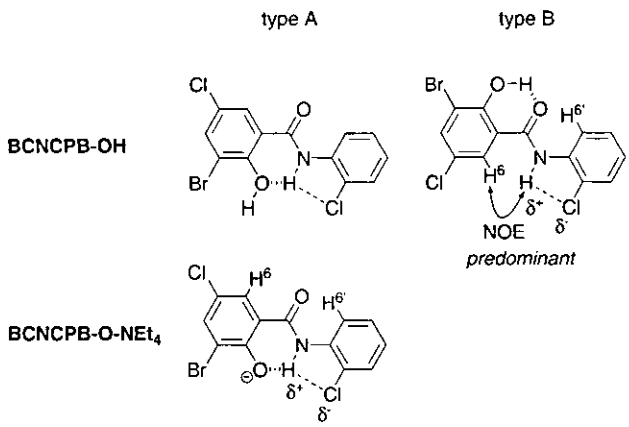

Chart 4. Solution structures of **BCNCPB–OH** and **BCNCPB–O–NEt$_4$**.

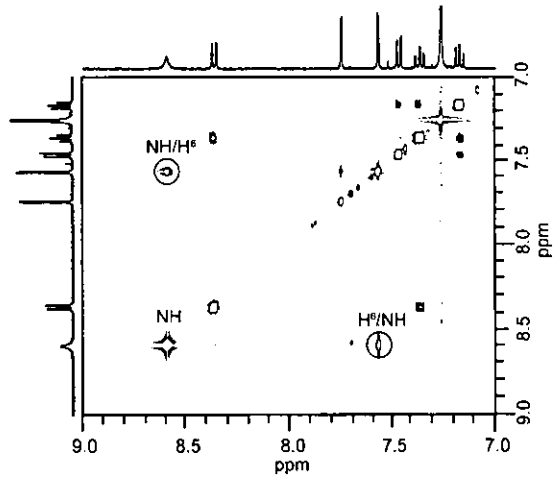

Fig. 4. NOESY spectrum of **BCNCPB–OH** in $CDCl_3$.

thought that the location of Cl2 is controlled by the same interactions. **BCNCPB–O–NEt$_4$** has an amide NH band at 3016 cm^{-1}, which is a very low frequency for ν(NH) even if the NH proton forms a hydrogen bond, (NH···O(H)[28] 3390 cm^{-1}, NH···O(Ac)[29] approximately 3400 cm^{-1}, NH···O(carboxylate)[28] 3024 cm^{-1}, NH···O(phosphate)[30] 3226 cm^{-1}, etc.) and shows that the NH···O(oxyanion) hydrogen bond fomed in **BCNCPB–O–NEt$_4$** is very strong. The ν(NH) shift in **BCNCPB–O–NEt$_4$** is comparable to that in the sodium salt of 3,5-dibromosalicylanilide,[20] which appears at 3000–2900 cm^{-1}.

Solution Structures of BCNCPB–OH and BCNCPB–O–NEt$_4$. Figure 3a shows the ^{1}H NMR spectrum of **BCNCPB–OH** in $CDCl_3$. A phenolic OH signal was observed at 12.0 ppm, which is shifted to a very low field compared to non-hydrogen bonded phenolic OH (4–6 ppm), indicating the formation of a OH···O=C hydrogen bond (type B in Chart 4) similar to the solid state. An amide NH signal was observed at 8.6 ppm, which is slightly downfield compared to δ(NH) in non-hydrogen bonded benzamide (6–8 ppm), showing that the weak NH···Cl hydrogen bond established in the solid state is maintained in solution. A NOE correlation between the NH and the 6-positioned aryl proton (H^6 at 7.6 ppm) was observed, but not between the NH and 6′-positioned aryl proton (H$^{6'}$ at 8.4 ppm) in the NOESY spectrum (Fig. 4). These results also support the type B conformation. On the other hand, a minor conformer in addition to type B was established in the IR results because of its higher time resolution than ^{1}H NMR. **BCNCPB–OH** gives NH stretching bands at 3425 and 3357 cm^{-1} (Fig. 5a). The ratio of each of the conformers was estimated to be about 90 and 10%, respectively, from the ratio of the area of the bands. The predominant band is assigned to the type B conformer (3416 cm^{-1} in the solid state). The NH band at 3357 cm^{-1} is assigned to the NH···O hydrogen bonded conformer (type A).[18,29] The band at high frequency, 3483 cm^{-1}, is assigned to ν(OH) in the type A conformation.[20] The OH band in the type B conformation was not observed in the spectrum because of line broadning.[20]

In the ^{1}H NMR spectrum of **BCNCPB–O–NEt$_4$** (Fig. 3b), an amide NH signal was observed at 15.2 ppm, which is downfield compared to the non-hydrogen bonded NH, indicating the formation of a strong NH···O(oxyanion) hydrogen bond (type A) similar to the solid state. The NH shows no NOE correlation with other protons in the NOESY spectrum (data not shown). It also supports the type A conformation. The IR results (Fig. 5b), where an NH band was observed at 3015

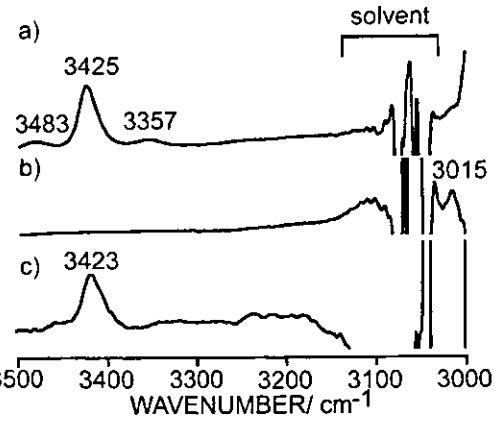

Fig. 5. IR spectra of 5 mM CH_2Cl_2 solution of **BCNCPB–OH** (a), **BCNCPB–O–NEt$_4$** (b), and BH3I-2′ (c).

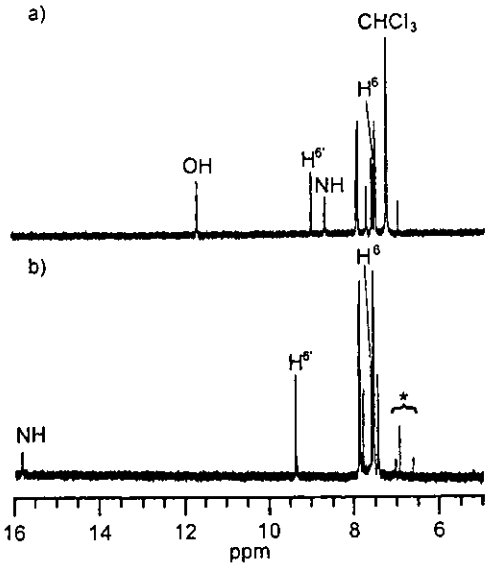

Fig. 6. ^{1}H NMR spectra of BH3I-2′ in $CDCl_3$ (a) and deprotonated BH3I-2′ in CD_3CN (b).

cm^{-1}, also show strong NH···O(oxyanion) hydrogen bonding.

Solution Structures of BH3I-2′. Figure 6a shows the ^{1}H NMR spectrum of BH3I-2′. Phenolic OH and amide NH signals were observed at 11.7 and 8.7 ppm, respectively. These similar chemical shifts to **BCNCPB–OH** show that BH3I-2′ has similar hydrogen bonds (Chart 5). An observed NOE correlation between the NH and the 6-positioned aryl proton (H^6 at 7.5 ppm) supports the type B conformation (Fig. 7). However, BH3I-2′ gives one NH band at 3423 cm^{-1} in the IR spectrum that is different from **BCNCPB–OH** (Fig. 5c). This is because iodine acts as a weaker hydrogen bonding accepter (OH···I) compared to bromine due to a smaller electronegativity. BH3I-2, which has bromine, probably has a minor conformer similar to **BCNCPB–OH**.

In the ^{1}H NMR spectrum of deprotonated BH3I-2′ (Fig. 6b), an amide NH signal was observed at 15.8 ppm, which is extremely downfield, similar to **BCNCPB–O–NEt$_4$**. This indicates NH···O(oxyanion) hydrogen bonding (type A). The type A conformation is also supported by the disappearance of the

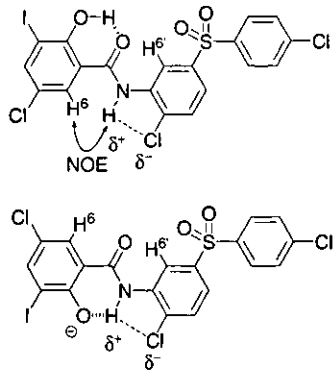

Chart 5. Solution structures of protonated and deprotonated forms of BH3I-2′.

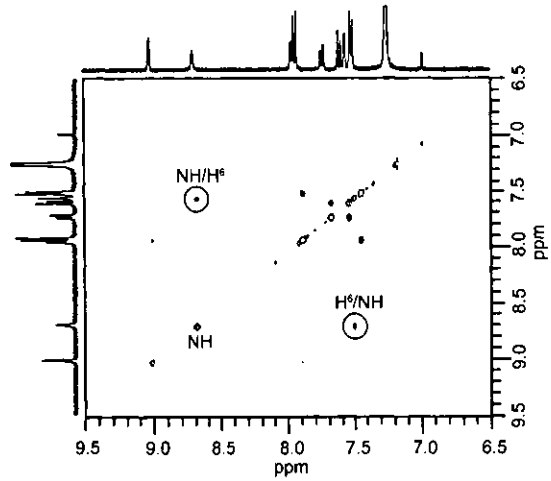

Fig. 7. NOESY spectrum of protonated BH3I-2′ in $CDCl_3$.

NOE correlation regarding NH.

Protonated and deprotonated BH3I-2′ form similar hydrogen bonds to the predominant conformations of **BCNCPB–OH** and **BCNCPB–O–NEt$_4$**, respectively. BH3I-2 probably prefers similar conformations.

pK_a of BCNCPB–OH in an Aqueous Micellar Solution. The pH titration of **BCNCPB–OH** was performed in an aqueous micellar solution. Under these conditions, **BCNCPB–OH** is incorporated into the hydrophobic layer where the hydrogen bonds are supported. These conditions also realize a hydrophobic cleft formed in Bcl-xL where BH3I-2 binds.[1] The titration method using an aqueous micellar solution is adequate to mimic the hydrophobic environments inside of protein.[23,24] Because protons can move inside and outside of micelles freely, the pK_a value of **BCNCPB–OH** is evaluated by pH measurements in the aqueous layer. **BCNCPB–OH** exists inside micelles due to its poor solubility in water during the titration. The pK_a value of **BCNCPB–OH** obtained from the titration was 5.1, which is very low compared with phenol (9.9 in water[31]). In addition to the electron-withdrawing effect of Cl, Br, and the aryl *N*-substituent (Ar_B), the existence of amide NH, which forms an intramolecular NH···O(oxyanion) hydrogen bond in the deprotonated form, lowers the pK_a value.[19,23,28] The pK_a value of BH3I-2 should be equal to or slightly less than 5.1 because an additional electron withdrawing substitu-

ent, the 4-chlorophenylsulfonyl group on the *N*-2-chlorophenyl group, of BH3I-2 has little effect on its acidity.[11]

Proposed Binding Structure of BH3I-2. The structure of the BH3I-2/Bcl-xL complex has been computationally proposed using the solution structure of the BakBH3–peptide/Bcl-xL complex.[1,21,22] This is based on the fact that the structure of Bcl-xL and the inhibitor-binding site are similar to those of the BakBH3–peptide/Bcl-xL complex. In this complex, BH3I-2 binds to a hydrophobic cleft formed by the BH1, BH2, and BH3 regions. The 3-positioned bromine interacts with the side chain of Tyr65 and the 5-positioned chlorine with the side chain of Phe61 and Phe110, etc. The presence of the interactions is demonstrated by a change in the inhibitory activity induced by the substitution of these halogen atoms. In the complex, the structure of BH3I-2 is represented in the protonated form and has an intramolecular NH···O hydrogen bond (type A). Our structural analysis of BH3I-2, however, shows that BH3I-2 forms an intramolecular OH···O=C hydrogen bond (type B) in the protonated form. It is difficult to fit BH3I-2 into the hydrophobic cleft while keeping the intramolecular OH···O=C hydrogen bond and the interactions between bromine–Tyr65, chlorine–Phe110, and chlorine–Phe61, because the chlorine on the *N*-aryl ring would be too close to the side chain of Phe61 or Ala106 under this assumption (Fig. 8b). On the other hand, it is reasonable that BH3I-2 binds in the deprotonated form in which an intramolecular NH···O(oxyanion) hydrogen bond is formed (Fig. 8a). This suggestion is supported by the pK_a value of BH3I-2 of about 5.1, which indicates that BH3I-2 is deprotonated under physiological conditions (pH = 7.2).[2] It is possible that Tyr65 does not interact with bromine but forms an intermolecular OH(Tyr)···O(oxyanion) hydrogen bond.

Different from other salicylamide inhibitors noted above, BH3I-2 binds to the protein in deprotonated form. This is because the pK_a value of BH3I-2 is lower than others due to strong electron-withdrawing substituents (Cl ($\sigma_{para} = 0.23$) and Br ($\sigma_{para} = 0.23$)) compared to others (F ($\sigma_{para} = 0.06$) or NHCHO ($\sigma_{para} = 0.00$)).[25]

Conclusion

In this study, BH3I-2 models, **BCNCPB–OH** and **BCNCPB–O–NEt$_4$**, were synthesized and structurally analyzed. The presence of an intramolecular OH···O=C hydrogen bond in **BCNCPB–OH** and an intramolecular NH···O(oxyanion) hydrogen bond in **BCNCPB–O–NEt$_4$** as established by X-ray analyses and IR spectra. The ^{1}H NMR and IR results of **BCNCPB–O–NEt$_4$** have revealed that the structure in the solid state is maintained in dilute solution with similar hydrogen bonds. **BCNCPB–OH** prefers a similar conformation to the solid state predominantly, but has a minor conformer having an NH···O hydrogen bond. ^{1}H NMR and IR spectra show that the protonated and deprotonated BH3I-2′ form intramolecular hydrogen bonds in the same manner as the corresponding models except for no evidence of the minor conformers in the protonated form. The deprotonation of BH3I-2 in the BH3I-2/Bcl-xL complex is suggested by the low pK_a value of **BCNCPB–OH**. It is also supported by the possible OH(Tyr)···O(oxyanion) hydrogen bond formation between the OH group of Tyr65 and the phenoxy oxygen atom of BH3I-2.

Experimental

Materials. BH3I-2′ was purchased from CALBIOCHEM. Other reagents were purchased from Nacalai Tesque or Tokyo Chemical Industry and used without further purification. All organic solvents were dried over CaH_2 and distilled under an Ar atmosphere before use.

Synthesis. 3-Bromo-5-chloro-2-hydroxybenzoic Acid (1): This compound was prepared using a modified method reported in the literature.[32]

To a solution of 3-bromo-5-chloro-2-hydroxybenzaldehyde (278 mg, 1.3 mmol) in dioxane (15 mL) were added NaH_2PO_4 (800 mg, 5.1 mmol) in water (5 mL) and sulfamic acid (186 mg, 1.92 mmol). The reaction mixture was cooled to 7 °C and then NaClO2 (186 mg, 1.7 mmol) in water (0.7 mL) was added gradually while keeping the temperature below 10 °C. The reaction mixture was stirred for 30 min below 10 °C. Sodium sulfite (195 mg, 1.5 mmol) was added with stirring for 15 min below 10 °C. Hydrochloric acid was added until a pH of 1 was obtained. Volatile materials were evaporated, and the resulting solution was cooled to deposit a white precipitate, which was collected by filtration and washed with water (309 mg, 94%).

Anal. Found: C, 33.37; H, 1.63%. Calcd for $C_7H_4BrClO_3$: C, 33.43; H, 1.60%. Mp: 238–239 °C. ^{1}H NMR (DMSO-d_6; TMS) δ 7.91 (1H, m, Ar–H), 7.74 (1H, m, Ar–H). ^{13}C NMR (DMSO-d_6): δ 170.3, 156.7, 137.3, 128.7, 122.8, 115.3, 111.3. ESI-MS:

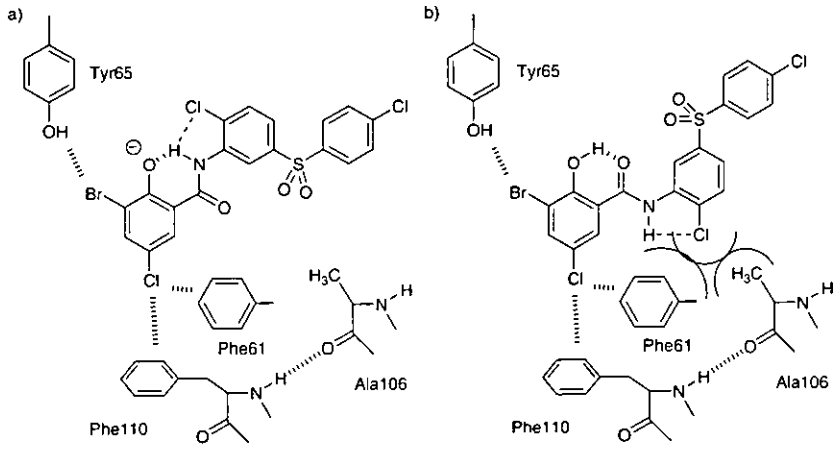

Fig. 8. Proposed binding structure in type A conformation (a) and type B conformation (b).

$(M - H^+)^-$, 249.1 (calcd for $M - H^+$; 248.90).

2-Acetoxy-3-bromo-5-chlorobenzoic Acid (2): 3-Bromo-5-chloro-2-hydroxybenzoic acid (519.3 mg, 2.1 mmol) was dissolved in 10 mL of THF. To the solution was added acetyl chloride (0.15 mL, 2.1 mmol), followed by triethylamine (0.3 mL, 2.2 mmol). The reaction mixture was stirred overnight, and the white precipitate was then filtered out. The filtrate was concentrated under reduced pressure. The resultant white powder was used without further purification (555 mg, 92%).

Mp: 153–155 °C. ^{1}H NMR ($CDCl_3$; TMS) δ 8.01 (1H, d, J = 2.4 Hz, Ar–H), 7.83 (1H, d, J = 2.4 Hz, Ar–H), 2.38 (3H, s, CH_3). ^{13}C NMR ($CDCl_3$): δ 168.0, 167.6, 147.3, 137.5, 132.1, 131.2, 125.1, 119.5, 20.7. ESI-MS: $(M - H^+)^-$, 290.9 (calcd for $M - H^+$; 290.91).

2-(2-Chlorophenylcarbamoyl)-6-bromo-4-chlorophenyl Acetate (3): 2-Acetoxy-3-bromo-5-chlorobenzoic acid (319 mg, 1.1 mmol) and triethylamine (0.20 mL, 1.4 mmol) were dissolved in 40 mL of THF. The solution was cooled to −20 °C. To the solution was added isobutyl chloroformate (IBCF) (0.18 mL, 1.4 mmol) gradually, keeping the temperature under −15 °C. After stirring for 5 min, *o*-chloroaniline (0.15 mL, 1.4 mmol) in THF (4 mL) was dropped into the reaction mixture. The reaction mixture was stirred for 1 h at −15 °C, and then 2 days at room temperature. The solvent was removed, and the residue was extracted with ethyl acetate and washed with 2% HCl aq., 4% $NaHCO_3$ aq., and sat. NaCl aq., and then dried over anhydrous sodium sulfate. The removal of the solvent gave a brown oily residue. The reprecipitation from diethyl ether/hexane gave a white powder. Recrystallization from ethyl acetate/hexane gave colorless needles (169 mg, 62%).

Mp: 128–129 °C. ^{1}H NMR ($CDCl_3$; TMS) δ 8.54 (1H, s, NH), 8.49 (1H, d, J = 7.6 Hz, Ar_B–H), 7.85 (1H, d, J = 2.4 Hz, Ar_A–H), 7.76 (1H, d, J = 2.4 Hz, Ar_A–H: protons on phenolic moiety), 7.41 (1H, dd, J = 8.4, 1.6 Hz, Ar_B–H: protons on *N*-aryl group), 7.33 (1H, t, J = 8.4 Hz, Ar_B–H), 7.09 (1H, dt, J = 7.6, 1.6 Hz, Ar_B–H), 2.41 (3H, s, CH_3). ^{13}C NMR ($CDCl_3$) δ 167.6, 161.1, 144.3, 135.6, 134.1, 132.8, 131.2, 129.4, 129.1, 127.9, 125.4, 122.9, 121.8, 118.9, 21.0. ESI-MS: $(M - H^+)^-$, 399.7 (calcd for $M - H^+$; 399.91).

3-Bromo-5-chloro-*N*-(2-chlorophenyl)-2-hydroxybenzamide (BCNCPB–OH): 2-(2-chlorophenylcarbamoyl)-6-bromo-4-chlorophenyl acetate (169 mg, 0.42 mmol) was dissolved in a mixture of MeOH (2 mL) and 1 M NaOH aq. (1 mL). The solution was stirred for two days and acidified by 2% HCl aq. The precipitated white powder was collected by filtration and recrystallized from THF/hexane. Colorless needles were obtained (34 mg, 23%).

Anal. Found: C, 43.23; H, 2.20; N, 3.83%. Calcd for $C_{13}H_8BrCl_2NO_2$: C, 43.25; H, 2.23; N, 3.88%. Mp: 157–160 °C. ^{1}H NMR ($CDCl_3$; TMS) δ 12.02 (1H, s, OH), 8.59 (1H, s, NH), 8.36 (1H, dd, J = 8.4, 1.6 Hz, Ar_B–H), 7.74 (1H, d, J = 2.4 Hz, Ar_A–H), 7.56 (1H, d, J = 2.4 Hz, Ar_A–H), 7.46 (1H, dd, J = 7.6, 1.6 Hz, Ar_B–H), 7.36 (1H, dt, J = 8.4, 1.6 Hz, Ar_B–H), 7.16 (1H, dt, J = 7.6, 1.6 Hz, Ar_B–H). ^{13}C NMR ($CDCl_3$) δ 165.9, 156.4, 137.2, 133.0, 129.2, 127.8, 126.0, 124.9, 124.2, 121.1, 122.4, 116.4, 113.4. ESI-MS: $(M - H^+)^-$, 358.1 (calcd for $M - H^+$; 357.90).

Tetraethylammonium 2-Bromo-4-chloro-6-[*N*-(2-chlorophenyl)carbamoyl]phenolate (BCNCPB–O–NEt$_4$): 3-Bromo-5-chloro-*N*-(2-chlorophenyl)-2-hydroxybenzamide (44.9 mg, 0.12 mmol) was dissolved in 8 mL of methanol. To the solution was added a 25% tetraethylammonium hydroxide aqueous solution (0.09 mL). The solution was stirred for 1 h, and solvents were removed under reduced pressure. The residue was washed with 10 mL of diethyl ether twice. The resultant powder was recrystallized from THF/diethyl ether to give **BCNCPB–O–NEt$_4$** as hygroscopic yellow crystals.

Anal. Found: C, 50.45; H, 5.52; N, 5.56%. Calcd for $C_{21}H_{27}BrCl_2N_2O_2 + (H_2O)_{0.5}$: C, 50.52; H, 5.65; N, 5.61%. Mp: 108–111 °C. ^{1}H NMR (CD_3CN; TMS) δ 15.22 (1H, s, NH), 8.70 (1H, dd, J = 8.0, 1.6 Hz, Ar_B–H), 7.77 (1H, dd, J = 3.2, 0.8 Hz, Ar_A–H), 7.40 (1H, dd, J = 7.6, 1.6 Hz, Ar_B–H), 7.39 (1H, d, J = 3.2 Hz, Ar_A–H), 7.25 (1H, tt, J = 8.0, 1.6 Hz, Ar_B–H), 6.96 (1H, tt, J = 7.6, 1.6 Hz, Ar_B–H), 3.14 (8H, q, J = 7.6 Hz, 4 × CH_2CH_3), 1.19 (12H, tt, J = 7.6, 2.0 Hz, 4 × CH_2CH_3). ^{13}C NMR (CD_3CN) δ 167.5, 167.2, 139.2, 134.7, 130.1, 129.4, 128.0, 123.8, 123.7, 123.1, 120.1, 119.1, 112.5, 53.1, 7.6.

Deprotonation of BH3I-2′. BH3I-2′ (1.5 mg, 2.8 μmol) was dissolved in 2 mL of THF. To the solution was added one drop of 25% tetraethylammonium hydroxide aqueous solution. The solution was then concentrated in vacuo. The residue was washed with 2 mL of diethyl ether and dried in vacuo.

^{1}H NMR Results of BH3I-2′ and Deprotonated BH3I-2′. BH3I-2′: ^{1}H NMR ($CDCl_3$; TMS) δ 11.70 (1H, s, OH), 9.01 (1H, d, J = 2.0 Hz, Ar_B–H), 8.69 (1H, s, NH), 7.96 (1H, d, J = 2.4 Hz, Ar_A–H), 7.93 (2H, d, J = 8.8 Hz, Ar_C–H: protons on *p*-chlorophenyl group), 7.73 (1H, dd, J = 8.8, 2.0 Hz, Ar_B–H), 7.60 (1H, d, J = 8.8 Hz, Ar_B–H), 7.56 (1H, d, J = 2.4 Hz, Ar_A–H), 7.52 (2H, d, J = 8.8 Hz, Ar_C–H).

Deprotonated BH3I-2′: ^{1}H NMR (CD_3CN; TMS) δ 15.85 (1H, s, NH), 9.41 (1H, d, J = 2.4 Hz, Ar_B–H), 7.90 (2H, d, J = 9.2 Hz, Ar_C–H), 7.82 (1H, d, J = 2.8 Hz, Ar_A–H), 7.63 (1H, d, J = 2.8 Hz, Ar_A–H), 7.58 (1H, d, J = 8.4 Hz, Ar_B–H), 7.57 (2H, d, J = 9.2 Hz, Ar_C–H), 7.46 (1H, dd, J = 8.4, 2.4 Hz, Ar_B–H), 3.14 (8H, q, J = 7.6 Hz, 4 × CH_2CH_3), 1.19 (12H, tt, J = 7.6, 2.0 Hz, 4 × CH_2CH_3).

Physical Measurements. ^{1}H NMR spectra in a $CDCl_3$ or CD_3CN solution were recorded on a JEOL GSX 400 spectrometer and a JEOL JNM EX 270 at 30 °C. NOESY spectra were recorded on a Varian UNITYplus 600 MHz spectrometer at 30 °C. Tetramethylsilane was used as a standard (0 ppm). ^{13}C NMR spectra in $CDCl_3$, CD_3CN, and DMSO-d_6 were recorded on a JEOL JNM EX 270 and Varian UNITYplus 600 MHz at 30 °C. Signals of the solvent were used as a standard {77.0 ppm ($CDCl_3$), 118.2 ppm (CD_3CN), and 39.7 ppm (DMSO-d_6)}. ESI-MS measurements were performed on a Finnigan MAT LCQ ion trap mass spectrometer in a methanol solution. IR spectra were recorded on a Jasco FT/IR 8300 spectrometer. Samples were prepared as Nujol mulls and in CH_2Cl_2 solution (1 and 5 mM).

pH Titration. The pH of a 10 mM **BCNCPB–OH** solution was determined using a Metrohm 716 DMS titrino, which is combined with a Metrohm 728 stirrer and a saturated calomel LL micro pH glass electrode. The saturated calomel micro glass electrode was calibrated with a 0.05 M $KHC_6H_4(COO)_2$ buffer (pH = 4.01), and a 0.025 M KH_2PO_4–Na_2HPO_4 buffer (pH = 6.86) at 30 °C. **BCNCPB–OH** was dissolved in a small amount of THF, and to this solution was added Triton X-100. The solution was concentrated to remove THF. The obtained residue was diluted with degassed water to give a micellar solution. The final concentration was a 10% Triton X-100 aqueous solution containing 10 mM of **BCNCPB–OH**. The solution was titrated with 0.1 M NaOH aq. at 30 °C. The pK_a value was estimated by the following equation:[23,24] $pK_a = pH - \log[Na^+] + \log\{[phenol]_0 - [Na^+]\}$.

X-ray Structure Determination. Each single crystal of **BCNCPB–OH** and **BCNCPB–O–NEt$_4$** was mounted in a loop